Sodium NMR Relaxation Parameters in Cartilage: Implications for MR Imaging

by

Adil Bashir

B.S., University of Engineering and Technology
Lahore, Pakistan (1991)

Submitted to the Department of Electrical Engineering
and Computer Science in partial fulfillment of the require-
ments for the degree of

Master of Science in Electrical Engineering

at the

MASSACHUSETTS INSTITUTE OF TECHNOLOGY

February 1995

© Massachusetts Institute of Technology, 1995. All Rights Reserved.

Author ....
Department of Electrical Engineering and Computer Science
February 10, 1995

Certified by ....
Deborah Burstein
Thesis Supervisor

Certified ....
Martha L. Gray
Thesis Supervisor

Accepted by ....
Frederic R. Morgenthaler
Chairman, Departmental Committee on Graduate Students

Sodium NMR Relaxation Parameters in Cartilage: Implications for MR Imaging

by

Adil Bashir

Cartilage is a dense connective tissue which covers the opposing ends of bones in a joint and acts as lubricating and resilient surface. Cartilage consists of hydrated extracellular matrix and relatively few cells. The extracellular matrix is a network of collagen fibers and large proteoglycan aggregates. Proteoglycans have a net negative charge under physiological conditions known as fixed charge density (FCD). These negatively charged molecules preferentially attract positive sodium ions and thus are a source of osmotic pressure which gives cartilage its resilience to compression. These extracellular sodium cations can be measured by nuclear magnetic resonance (NMR) and used as a nondestructive technique to monitor the tissue glycosaminoglycan concentration. Arthritis is a degenerative disease of cartilage and is characterized by a decrease in proteoglycan concentration. Sodium MR imaging can be an early indicator of this degenerative process and may provide non-invasive means of measuring cartilage degradation in vivo. The essential parameters which effect the signal intensity in sodium MRI are sodium density, and sodium T_1 and T_2 relaxation times. Therefore the main goal of the present study was to determine these relaxation parameters. Calf epiphyseal (EP) cartilage was harvested from distal ulna joints. T_1 determined for calf EP cartilage consisted of a single exponential time constant with mean of 18.2 ms and increased to 33.0 ms after trypsin degradation to remove cartilage proteoglycans. Cartilage T_2 consisted of two well defined exponential components, T_2 fast = 0.96 ms and T_2 slow = 21.1 ms. After treating cartilage with trypsin the T_2 fast decreased considerably to 0.2 ms with slow component changing slightly to 24 ms. In summary, these data provide the fundamental tissue parameters necessary for designing magnetic resonance imaging protocols necessary for quantitative sodium density weighted images. These protocols will ultimately be useful in monitoring early degeneration of cartilage and in evaluating in vivo therapies.

Thesis Supervisors:

Deborah Burstein, Ph.D.
Associate Professor of Radiology
Beth Israel Hospital
Harvard Medical School

Martha L. Gray, Ph.D.
Associate Professor of Electrical and Medical Engineering
Department of Electrical Engineering and Computer Science
MIT and Harvard-MIT Division of Health Science and Technology

Acknowledgments

Table of Contents

List of Figures

List of Tables

Chapter 1

Introduction

Articular cartilage is a connective tissue covering the surfaces of the bones in a joint. The function of articular cartilage is to provide a smooth lubricating surface for joint motion and resilient surface for load bearing. Epiphyseal cartilage is found in young animals and is a prior tissue of long bones [Poole A.R. 1991]. Cartilage consists of relatively few cells and a hydrated extracellular matrix which is responsible for many biomechanical and chemical properties of the tissue [Grodzinsky A.J. 1983]. The extracellular matrix consists of a mesh of collagen fibers and large proteoglycan aggregates. The collagen network provides the tissue with shear and tensile strength. Both collagen and glycosaminoglycan (GAG) chains of proteoglycans contain chemical groups (carboxyl, amino and sulfate) which are ionized under physiological conditions. Collagen has roughly equal numbers of amino and carboxyl groups resulting in collagen having little or no net charge. For proteoglycans, the sulfate and carboxyl groups associated with glycosaminoglycans predominate, thus they provide proteoglycans and hence cartilage with a net negative charge. This negative charge is known as fixed charge density (FCD). These negatively charged molecules preferentially attract positive counter ions (Na^+) and thus are the source of osmotic pressure which gives cartilage resilience to compression [Buckwalter et al 1988, Maroudas A 1979].

Osteoarthritis is a degenerative disease of cartilage which involves inflammation and erosion of cartilage. While it may occour in young it is most common in elderly [Yelin E. 1992]. The cartilage degeneration results in general softening and inflammation of the tissue. Eventually complete erosion of the tissue cartilage occurs exposing the underlying bone. Cartilage degeneration starts by changes in extracellular matrix composition and

function. For example, the early event in osteoarthritis is a loss of cartilage proteoglycans which results in a reduction in swelling pressure and compressive stiffness as compared to healthy tissue [Venn and Maroudas 1977].

Diagnosis of the disease is hampered by the difficulty and lack of generally accepted methods for quantitative assessment of the disease, especially at an early stage. Evaluation of the disease is currently based on nonspecific and subjective clinical findings which include stiffness, fatigue, joint pain, swelling and tenderness. Evaluation of the integrity of cartilage and other tissues of the musculoskeletal system has also been obtained through a variety of other techniques. Historically, plain radiographs were used to assess the disease state. These radiographic techniques are of limited use because they allow only indirect assessment of cartilage such as joint space narrowing. Arthrography and computed tomography (CT) scanning has been fairly successful in the diagnosis of the disease but they require the use of intraarticular injection of contrast agent and ionizing radiation. [Ghelman B 1985]. Orthopedists usually use arthroscopy to confirm structural changes such as lesions. It is an invasive procedure and requires direct visualization of the internal joint structure. It is also not useful to determine the disease in early stages in which gross structural changes have not become visible and can be used only for a limited number of joints.

Efforts are now being made to use magnetic resonance imaging (MRI) to study the degenerative diseases of the musculoskeletal system. Magnetic resonance imaging (MRI) is particularly valuable because of its excellent soft tissue contrast, its multiplanar capability, and lack of ionizing radiation. Moreover it is completely noninvasive and excellent soft tissue contrast is available without the use of any contrast agents. Using proton MRI, many people have shown the ability of MRI to accurately delineate the anatomical structures in normal joints including cartilage [Lai et al 1984, Reicher et al 1985a].

An early feature of arthritis is the loss of proteoglycans from the extracellular matrix. McDevitt and Muir [1976] found that cartilage becomes more hydrated and that proteoglycans can be more easily extracted from osteoarthritic cartilage in dog knees suggesting that a decrease in the amount of proteoglycan aggregation in osteoarthritis. A significant reduction in glycosaminoglycan concentration has been observed in osteoarthritic cartilage as compared to normal [Venn and Maroudas 1977]. Compared with other changes in cartilage degradation, the loss of glycosaminoglycans is most pronounced and its concentration can drop to nearly zero. Several methods have been reported for measuring GAG content in cartilage. Some techniques such as chemical analysis completely destroys the cartilage [Antonopoulas 1964, Bitter and Muir 1962, and Farndale 1986]. While other nondestructive techniques (streaming potential [Maroudas et al 1969], radio-ion tracers [Maroudas and Thomas 1970]) give good estimates of FCD and GAG content in vitro, these methods are not applicable for in vivo studies.

As described earlier the negatively charged glycosaminoglycans attract positive sodium counter ions. These extracellular sodium cations can be measured by nuclear magnetic resonance (NMR) spectroscopy and used as a nondestructive technique to monitor the tissue glycosaminoglycans. Recently Lesperance et al [1992] demonstrated that sodium magnetic resonance spectroscopy can be used as a nondestructive technique for monitoring the sodium concentration, and hence glycosaminoglycan content of articular and epiphyseal cartilage. If these results could be extended to imaging studies, it would provide a noninvasive means for the evaluation of early cartilage degradation. However in moving from spectroscopy to imaging some considerations need to be taken into account. Two important parameters for MR imaging are TR (repetition time between multiple excitations) and TE (echo time is the time between excitation of nuclei and signal acquisition). The signal saturates due to T_1 (longitudinal MR relaxation) effects if TR is less than $5T_1$,

and decays due to T_2 (transverse MR relaxation) effects during the echo time. This decay during TE can be substantial for sodium because the T_2 time constant has a component in the range of 0.5ms to 3ms for most biological systems and the echo times usually used in imaging are greater than 1ms.

The main goal of this project is to determine the T_1 and T_2 relaxation times of sodium in cartilage so that quantitative evaluation of Na concentration can be obtained from sodium MRI. These sodium images will reflect the proteoglycan content in cartilage. The specific aims for this study are:

(i) Determination of T_1 and T_2 relaxation times.

Variations in T_1 and T_2 within a tissue could complicate quantification of image intensity. Explanted samples of calf epiphyseal cartilage from distal ulna joints and articular cartilage from femoropatellar groove will be used to determine the sodium T_1 and T_2 relaxation times. The variability of relaxation times from tissue to tissue and position of explant will be determined.

(ii) Changes in relaxation times with pathologic interventions.

Cartilage samples will be treated with trypsin and Interleukin-1β (IL-1β) to mimic changes observed in arthritis. Treating the cartilage with trypsin cleaves the proteoglycan protein core, which allows the glycosaminoglycans to diffuse out of the tissue resulting in reduced tissue fixed charge density. Interleukin-1β is a cytokine and is thought to be involved in the destruction of cartilage matrix in rheumatoid arthritis and osteoarthritis. Treatment of viable cartilage with IL-1β results in a dose dependent release of proteoglycans. Relaxation times will be determined under these perturbations to normal cartilage.

(iii) Implications for MR imaging.

Image intensity in MRI is determined by sodium density, as well as the sodium T_1 relaxation time relative to the imaging parameter TR, and the T_2 relaxation time relative to the imaging parameter TE. Since it is not possible to determine the sodium relaxation times during imaging, average values for relaxation times must be used to calculate sodium concentration from image intensity. The measured variations in T_1 and T_2 between normal and diseased tissues will be used to determine the error in quantifying sodium concentration from the assumed T_1 and T_2 values for standard imaging parameters (TR and TE).

Chapter 2

Theory

In this chapter the basic principles of NMR spectroscopy and imaging are presented with emphasis on those applications more relevant for this study. The theory presented here is taken form the following texts. Stark and Bradley 1992, T.C. Farrar 1989, C.P. Slichter 1990, and C.H. Cho, J.P. Jones, and M. Shing 1993. The reader is referred to the above texts for more detailed analysis.

2.1 Basic Principles

Nuclei of atoms which contain an odd number of protons or neutrons or both possess nuclear magnetic moment $\vec{\mu}$ and angular momentum $\vec{J}$ which are related as given by equation 2.1

$$\vec{\mu} = \gamma \vec{J} \tag{2.1}$$

$$\vec{J} = \gamma I \hbar \tag{2.2}$$

where γ is the gyromagnetic ratio and is a fundamental property of the nucleus, I is the nuclear spin quantum number and $\hbar$ is the Planks constant divided by 2π. When such a nucleus is placed in a magnetic field the magnetic moment tries to align with the magnetic field just as a compass needle aligns with the magnetic field but the presence of angular momentum causes the magnetic moments to precess around the magnetic field. The equation of motion of a magnetic moment vector in a magnetic field $\vec{B}_o$ can be obtained by equating the rate of change of angular momentum to the torque

$$\frac{d\vec{J}}{dt} = \vec{\mu} \times \vec{B}_o \tag{2.3}$$

multiplying both sides of the above equation by γ gives us

$$\frac{d\vec{\mu}}{dt} = \gamma\vec{\mu} \times \vec{B}_o \qquad (2.4)$$

This equation describes the motion of a nuclear dipole moment when placed in a DC magnetic field. It can be summed over all magnetic moments to give us the equation of motion of net magnetization $\vec{M}$.

The frequency of precession of the nuclear dipoles about the magnetic field is often termed as Larmor frequency and is proportional to the applied field as given in equation 2.5, where γ for sodium is 11.26 MHz/Tesla and for protons is 42.6 MHz/Tesla.

$$\omega = \gamma\vec{B}_o \qquad (2.5)$$

With no external field applied i.e $\vec{B}_o = 0$, the thermal equilibrium situation can be represented as randomly distributed magnetic dipoles with net magnetization $\vec{M} = 0$. When the sample is placed in the magnetic field the magnetic dipoles align with the field (Figure 2.1). Quantum mechanics requires that the orientation of a magnetic dipole with respect to the applied field should be quantized. The number of allowed orientations is $2I + 1$ where I is the nuclear spin quantum number. For example hydrogen nuclei with spin equal to 1/2 are restricted to two orientations parallel (low energy state) and anti-parallel (high energy state) with the external field. The difference in the energy between these states is directly proportional to the applied field and is given as

$$\Delta E = \gamma\hbar\vec{B}_o. \qquad (2.6)$$

At thermal equilibrium (at room temperature) there is a small net excess of dipoles in the lower energy state, which corresponds to the parallel direction, resulting in a net magnetization $\vec{M}$ along the magnetic field (Figure 2.2).
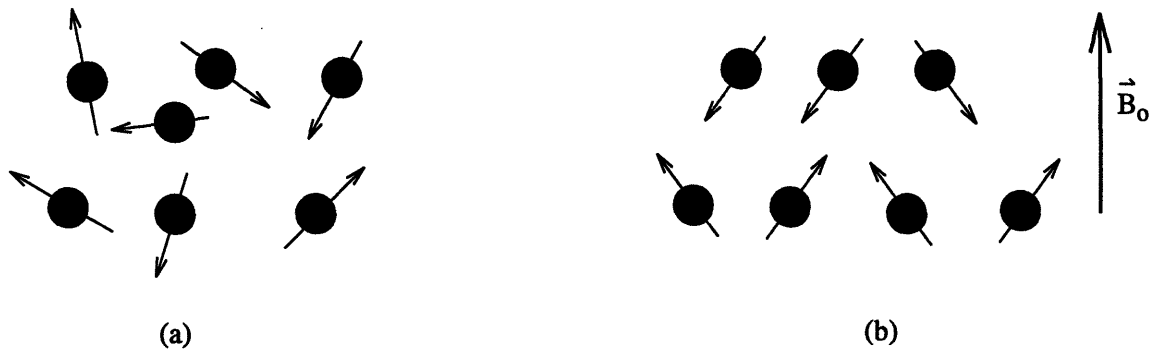
Figure 2.1: (a) In absence of magnetic field the moments are randomly distributed. (b) Application of an external magnetic field causes the moments to align parallel or anti-parallel to the external field.
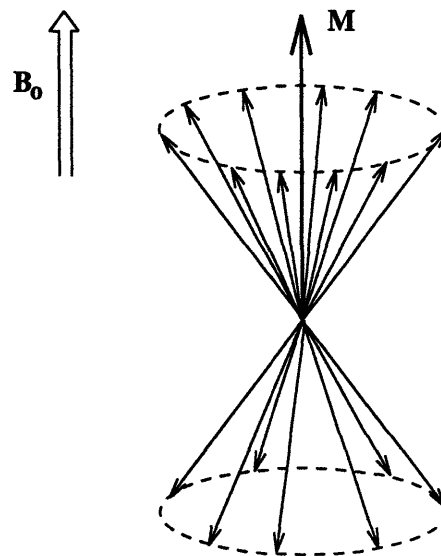
Figure 2.2: Vector representation of magnetization in the presence of an applied field. There is no net transverse magnetization due to the random phase of the magnetic moment vectors.

Now if energy in the form of a rotating magnetic field $\vec{B}_1$ with either its frequency equal to Larmor frequency or its energy equal to ΔE (both conditions are equivalent to each other as $E = \hbar\omega$) is applied it would equally likely *(i)* cause a nucleus initially in the lower energy state to absorb energy and make transition to the higher energy level or *(ii)* to stimulate the emission of energy by causing the transition of a nucleus initially in the higher energy state to the lower energy state. This $\vec{B}_1$ field is in the radio frequency (RF) range of MHz for biological applications and is usually referred to as RF pulse.

If there is a net excess of spins in lower energe state, as in thermal equilibrium, then absorption of energy takes place and some of the nuclei are promoted from low energy state to high energy state (Figure 2.3). This RF pulse also brings the phases of the magnetic moments into a coherent relationship. The effect is to cause the net magnetization $\vec{M}$ to rotate away from its equilibrium alignment along the z-axis.
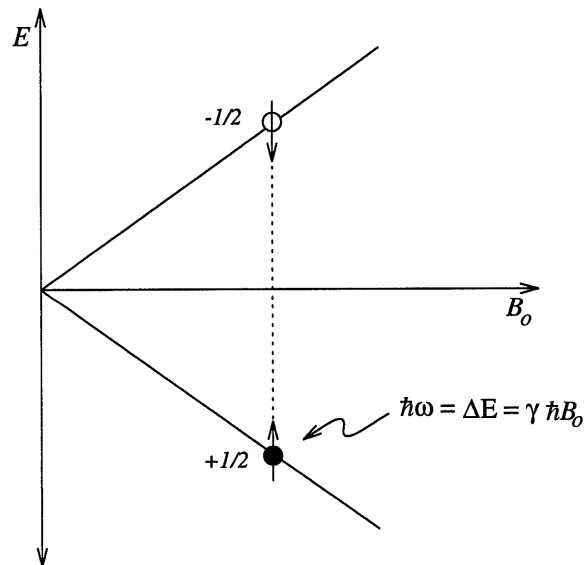
Figure 2.3: Energy level diagram for a spin $1/2$ system. The energy splitting increase linearly with applied field. Transitions between the two states can be induced by electromagnetic energy of frequency ω given by $\omega = \gamma B_o$.

The equation of motion for both DC magnetic field and RF excitation field is given as

$$\frac{d\vec{M}}{dt} = \gamma \vec{M} \times (\vec{B}_o + \vec{B}_1) \qquad (2.7)$$

If we define a rotating frame of reference in which the plane perpendicular to the static magnetic field $\vec{B}_o$ is rotating at Larmor frequency this rotation has an effect of creating a virtual field which causes the static field $\vec{B}_o$ to disappear from equation 2.7 and it reduces to

$$\frac{d\vec{M}}{dt} = \gamma \vec{M} \times \vec{B}_1 \qquad (2.8)$$

It is evident from equation 2.8 that the net magnetization $\vec{M}$ now precesses around the field $\vec{B}_1$ which is stationary in this rotating frame of reference. The basic process is summarized in figure 2.4. The angle by which $\vec{M}$ rotates is called the flip angle which depends on the magnitude and duration of the pulse and is given by the equation 2.9. A $\vec{B}_1$ pulse which tilts the magnitization $\vec{M}$ by 90° i.e from its lognituidinal equilibrium position to transverse plane is known as 90° RF pulse.

$$\theta = \gamma B_1 t = \omega t \qquad (2.9)$$

Once $\vec{M}$ is deflected and the field is switched off, $\vec{M}$ precesses about the direction of the main magnetic field ($\vec{B}_o$), with a component in the transverse plane. The precession of the transverse component of $\vec{M}$ induces a voltage in a receiver coil and this voltage constitutes the MR signal known as free induction decay or FID. For a single type of nucleus the FID has an exponentially decaying envelope whose Fourier transform is known as spectrum and is of Lorentzian shape. If rate of decay (FID) is slower the spectrum is more sharp and vice versa. The area under the spectrum is proportional to the number of nuclei in the sample.

With time following the excitation, the system will return to its thermal equilibrium after losing energy due to the relaxation process. There are two distinct types of relaxation; spin-lattice relaxation (T_1) and spin-spin relaxation(T_2). T_1 represents the time constant by which the net magnetization vector in the z direction returns to its initial value after it has been perturbed by th RF field. The time constant T_2 describes the decay of the transverse component of the magnetization.
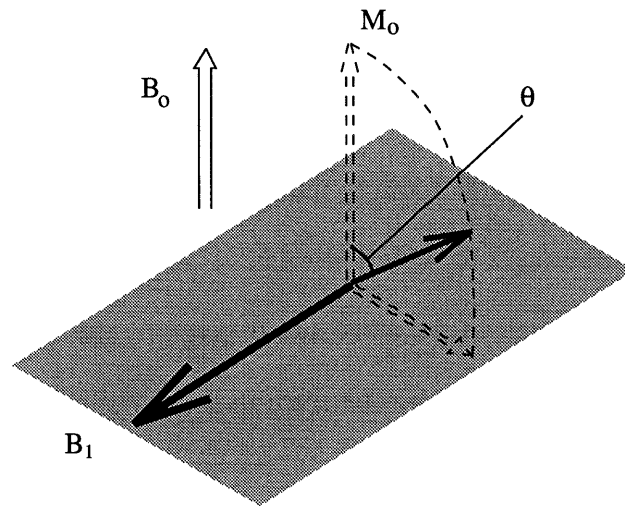
Figure 2.4: In presence of an exciting field B_1 the magnetization M_o in the rotating frame rotates about B_1 by an angle θ.

2.1.1 Sodium NMR

Thus far the theory of NMR has been presented in terms of spin $1/2$ nuclei whose magnetic moments align parallel or anti-parallel with the magnetic field. However the nucleus of sodium has a nuclear spin quantum number $I = 3/2$ which implies that there are four possible orientations of the sodium nucleus with respect to the static magnetic

field. These four quantum states are characterized by the magnetic quantum number m, which can take values $+3/2, +1/2, -1/2, -3/2$ with corresponding energies in the external $\vec{B}_o$ field equal to

$$E_m = -\gamma \hbar m \vec{B}_o \tag{2.10}$$

A distinguishing feature of sodium and other nuclei with spin greater than $1/2$ is their nuclear electric quadrupole moment. An electric quadrupole moment arises from an asymmetry of the distribution of the electric charges and does not depend on the exact charge. When this quadrupole moment interacts with the local electric field gradients it shifts the energy levels according to the square of the quantum number m, to a first approximation and is given by the following equation [Slichter 1990]

$$E_m = -\gamma \hbar B_o m + \frac{e^2 q Q}{4I(2I-1)}\left(\frac{3\cos^2\theta - 1}{2}\right)[3m^2 - I(I-1)] \tag{2.11}$$

where e = elementary charge, Q = nuclear quadrupolar moment, and q = electric field gradients. The energy level diagram in the presence of quadrupole interaction is shown in figure 2.5 The $m = \pm 3/2$ levels shift identically while the $m = \pm 1/2$ levels shift identically.

Transitions are only allowed between adjacent states. The central transition $I = -1/2 \leftrightarrow 1/2$ is unaffected by the quadrupolar moment to the first order and yield a relatively narrow signal with a transition probability of 0.4. The outer transitions occur with a probability of 0.3 each and are shifted to higher and lower frequencies. The transition energies due to quadrupole interaction depend on the orientation of the molecular symmetry axis relative to the external magnetic field. The position of the outer lines with respect to the center line is given by

$$\Delta\omega = \frac{e^2 q Q}{2}(3\cos^2\theta - 1) \tag{2.12}$$

29

Thus the seperation of outer lines relative to cental line varies with the orientation and the maximum splitting is observed when $\theta = 0$. Molecular motions cause fluctuations in electric field gradients and these fluctuations reduce the average quadrupole splitting. In biological systems where the nuclei are in fast isotropic motions the fluctations in electric field gradients averages out to zero and no line splitting is observed. Thus the frequency of the detected signal is the frequency which occurs in the absence of electric field gradients.

```
m = -3/2   ─────────────────·········-----

                ℏω₀                      ℏ(ω₀+Δω)      30%

m = -1/2   ─────────────·········‧‧‧‧‧

                ℏω₀                      ℏω₀           40%

m = +1/2   ─────────────·········‧‧‧‧‧

                ℏω₀                      ℏ(ω₀- Δω)     30%

m = +3/2   ─────────────·········-----

              (a)                         (b)
```
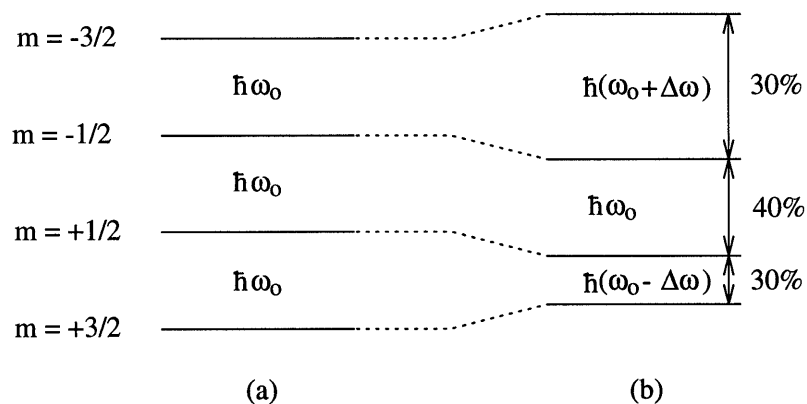
Figure 2.5: Energy level diagram for spin 3/2 nucleus. (a) Energy levels in presence of a static magnetic field. (b) Energy levels in presence of a static magnetic field and electric field gradient when the nucleus is under going quadrupolar interaction. The percentages of transition that occur between perticular levels are also represented.

2.2 NMR Relaxation

Net nuclear magnetism can be described by its longitudinal and transverse components. At equilibrium in a field B_0 , the transverse magnetization has a zero value. Application of $90°$ RF pulse at the Larmor frequency decreases the longitudinal nuclear magnetization and simultaneously produces a transverse magnetization. The stimulated

transition of energy by the sample is almost instantaneous as compared to relaxation processes. After the pulse, longitudinal and transverse magnetization reach their respective equilibrium values described as a exponential process with the time constants T_1 (spin-lattice or longitudinal relaxation time) and T_2 (spin-spin or transverse relaxation time).

2.2.1 Spin-Lattice Relaxation (T_1)

Once excited by the RF pulse the (excited) spins return to the ground state by dissipating their excess energy to the lattice (Figure 2.6). In order to dissipate energy to the lattice the spins must encounter a stimulating radiofrequency field fluctuating at the same rate as the precessional frequency of the spins. The fields causing this relaxation are provided by the rotational, vibrational and translational motions of atoms and molecules present in the lattice. These motions cause the interaction of the nuclear magnetic dipole and electric quadrupole moments with the surrounding atoms and enable energy transfer. Fluctuating fields at Larmor frequency are necessary for effective T_1 relaxation thus T_1 relaxation times are dependent on the precessional frequency hence on the strength of the external magnetic field.

2.2.2 Spin-Spin Relaxation (T_2 and T_2^*)

Transverse relaxation influences the rate of decay of the FID. After the RF pulse has tipped the nuclear magnetization towards transverse plane the individual spins comprising this vector precess together or "in phase". However, the precession does not remain in phase. Local differences in magnetic field strength cause some nuclei to precess at different rates from the others and the individual spins dephase and cancel each other out. In addition spins exchange energy with each other causing a randomization of phase. As a result the sum of nuclear magnetization vectors in the transverse plane decays to zero (Figure 2.6). The time constant of this decay is called T_2^*.

z

z

y'

x'

t = 0

y'

x'

spin-spin
relaxation

z

z

spin-lattice
relaxation

y'

x'

M_o

y'

x'

t = ∞
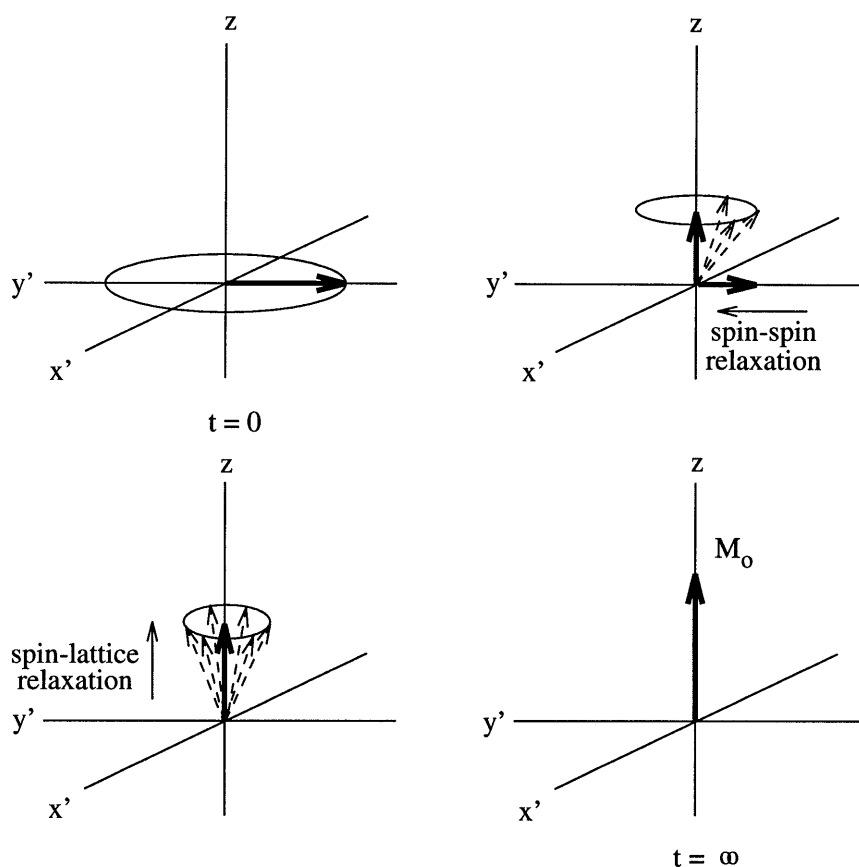
Figure 2.6: After a 90° pulse at $t = 0$ the longitudinal magnetization grows towards z-axis by T_1 relaxation and the transverse magnetization (T_2) decays in the x'y' plane by dephasing of individual spins shown dotted (only excess of spins for low energy state are shown).

As only the net transverse magnetization is responsible for the production of the NMR signal, it is T_2^* that is responsible for the decay of the detectable signal (the envelope of the FID) and it is related to the linewidth at half height (Figure 2.7) of the signal by the relation

$$\Delta \upsilon_{1/2} = 1/\left(\pi T_2^*\right)$$ (2.13)

The spin exchange relaxation time is referred to as T_2. Since this parameter is a result of energy interchange between spinning nuclei it is known as "spin-spin" relaxation. T_2 is

longer than T_2^* because it does not contain contribution form static magnetic field inhomogeneities. If the magnetic field inhomogeneities remain constant over the period of data acquisition their contribution to the loss of signal decay can be made reversible by generating spin echos (described later). If a sequence of spin echos are generated the FID and individual spin echos decay with a time constant T_2^*, but the peak heights of successive spin echos decay with a time constant equal to T_2.
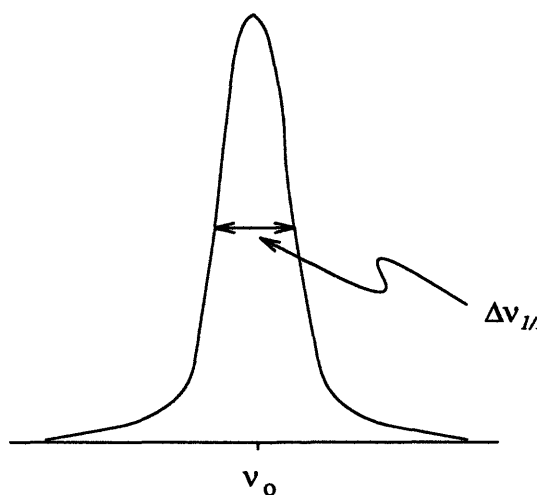
Figure 2.7: A typical spectrum with $\Delta v_{1/2} = 1/\left(\pi T_2^*\right)$. The area under the spectrum is proportional to the number of nuclei in the sample.

2.3 NMR Relaxation Mechanisms

Any mechanism that gives rise to fluctuating fields at the nucleus can produce relaxation, but the two major relaxation mechanisms are nuclear dipolar relaxation and electric quadrupolar relaxation.

2.3.1 Dipole-Dipole Relaxation

In case of spin $1/2$ nuclei such as protons the dominant relaxation mechanism is the magnetic dipole-dipole interactions between the nucleus and the magnetic moments in the

surrounding atoms. These interactions depend on the magnitudes of the interacting nuclear magnetic dipole moments, the relative position of the nucleus under consideration and its surroundings. As shown in figure 2.8 the local magnetic field present at nucleus B due to nucleus A is [Farrar 1989]

$$B_{loc} = \frac{\mu_A (3\cos^2\theta - 1)}{r_{AB}^3}$$
(2.14)

where r_{AB} is the distance between nuclei A and B and θ is the angle between the position vector of nuclei A and B and the external field. θ and r_{AB} are time dependent due to rotational and vibrational motions.

T_1 and T_2 relaxation times both depend on molecular motions which are usually expressed in terms of correlations times (τ_c). Molecules are constantly vibrating, rotating and colliding into each other and the correlation time is defined as the minimum time a molecule spends in a particular state. The rotational correlation time is the time required to change the angle θ, and the vibrational correlation time is defined as the time in which r_{AB} changes appreciably. Associated with correlation time is a correlation function which describes the average behaviour of the molecular motions.
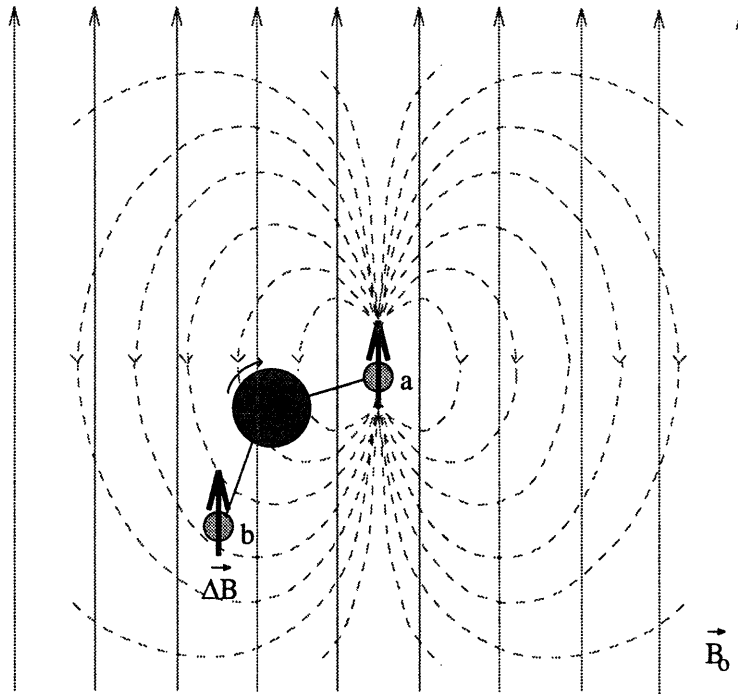
Figure 2.8: Dipole dipole coupling between two water protons. Solid lines represent the static magnetic field $\vec{B}_o$, the dashed lines represent the local field due to the dipole moment of proton a. Proton b experiences a small local perturbation $\Delta\vec{B}$ due to the presence of proton a. As water molecule vibrates and rotates the magnitude and direction of this local field changes.

The Fourier transform of the correlation function is defined as spectral density function, $J(\omega)$

$$J(\omega) \propto \frac{\tau_c}{1 + \omega^2 \tau_c^{\,2}}$$

(2.15)

For dipolar interactions the T_1 and T_2 relaxation rates can be expressed in terms of the spectral density function:

$$\frac{1}{T_1} \propto [J(\omega_0) + J(2\omega_o)]$$

(2.16)

$$\frac{1}{T_2} \propto [J(0) + J(\omega_o) + J(2\omega_o)]$$ (2.17)

Thus T_1 depends on molecular motions at high frequencies, ω_o and $2\omega_o$, and from figure 2.9 it can be seen that when the frequency matches the Larmour frequency ω_o, the more nuclei are contributing (propotional to shaded region) towards molecular motions in viscous liquids and the relaxation is most efficient. This dependence on Larmour frequency also makes T_1 dependent on field strengths. For solids and non-viscous liquids the motions at Larmour frequency does not possess much intensity and the spin lattice relaxation times are longer (Figure 2.10). T_2 relaxation has the same terms as T_1 with the addition of a zero frequency term corresponding to slow molecular motions. This makes T_2 less than or equal to T_1. For solids the molecular motions are dominant by slow fluctuations therefore $J(0) \gg J(\omega_o)$ and $J(2\omega_o)$ and spin-spin relaxation is more efficient (Figure 2.10).

By altering the temperature we can alter the correlation times and hence the frequency distributions of the molecular motions which can effect the relaxation times (Figure 2.10).
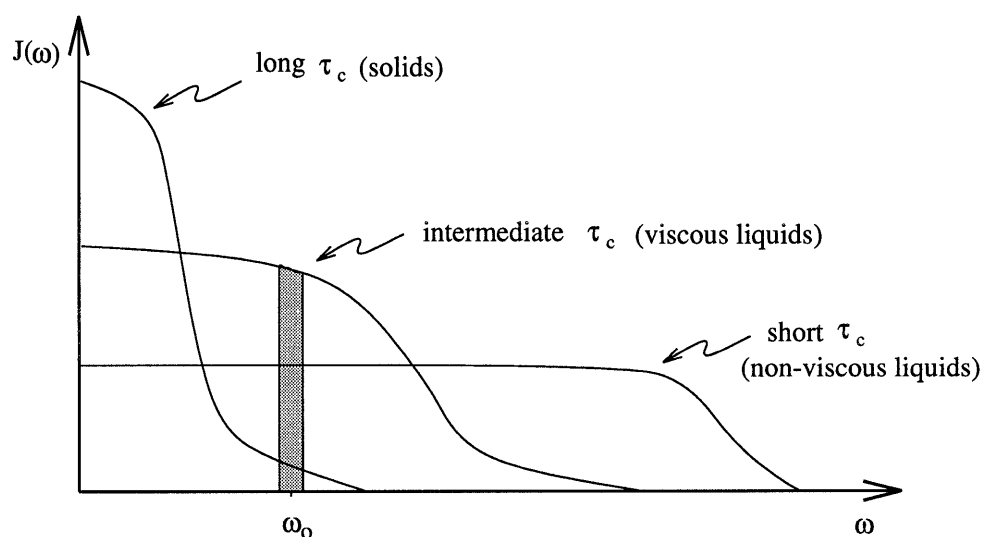
Figure 2.9: The spectral density function plotted for various values of correlation times
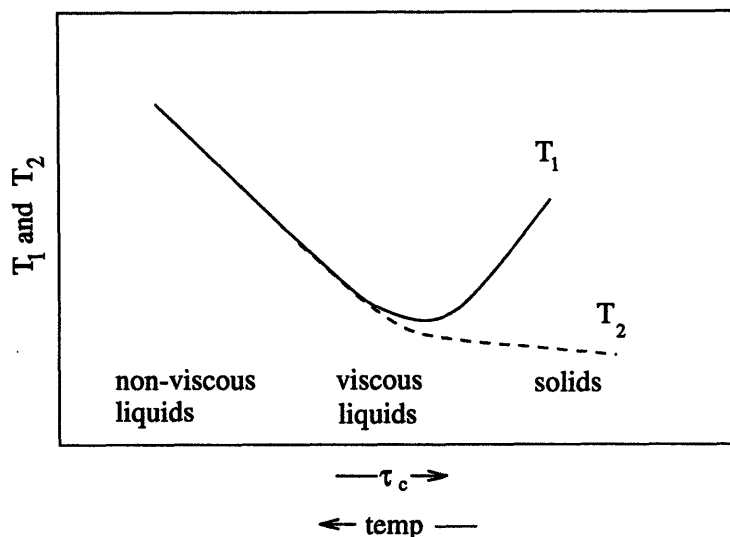
Figure 2.10: NMR relaxation time dependence on temperature and correlation time. When correlation time (τ_c) is close to inverse of Lamour frequency as in case of viscous liquids, more nuclei are participating in the relaxation process and the relaxation is more efficient. The T_2 for solids is smaller because for longer correlation times, low or zero frequency spectral density term is large and T_2 relaxation for solids is more efficient (eq 2.17).

2.3.2 Quadrupolar Relaxation

Nuclei with spin $1/2$ have a magnetic dipole moment but no electric quadrupole moment. Nuclei with spin greater than $1/2$ have both magnetic dipole moment and electric quadrupole moment. The electric quadrupole moment is a measure of asymmetry of the nucleus. This deviation from spherical shape causes a nucleus to be sensitive to local electric field gradients. The interaction of this quadrupole moment with electric field gradients results in nuclear electric quadrupole relaxation. This relaxation is generally much more efficient than dipolar relaxation resulting in much broader NMR lines.

The strength of the quadrupole moment is characterized by the product of the nuclear quadrupole moment eQ and the electric field gradient eq strength as shown in equation 2.11 where the electric field gradient is a complicated function of the surrounding environ-

ment, neighboring ions and surrounding electron distribution. Slichter [1990] and Pette-grew et al [1987] have shown that this quadrupole interaction is dependent on (1) the distance between nuclear electric quadrupole moment and the origin of the electrostatic field gradient tensor and is proportional to $1/r^3$, (2) the relative orientation of the electric field gradient tensor and the nuclear electric quadrupole moment given by the expression $3\cos^2\theta - 1$ and (3) the fluctuations in these quantities.

The relaxation due to quadrupolar interactions has been calculated by Hubbard [1970] and Bull et al [1973], who considered the case where the electric field gradients fluctuate less rapidly than the Larmor period of the nucleus. Both T_1 and T_2 relaxation expressions are biexponential due to transitions between different spin states. For T_1 relaxation the signal observed is given by

$$S_1(t) = 0.2e^{-(t/T_{1fast})} + 0.8e^{-(t/T_{1slow})} \tag{2.18}$$

for T_2 the signal is given by

$$S_2(t) = 0.6e^{-(t/T_{2fast})} + 0.4e^{-(t/T_{2slow})} \tag{2.19}$$

the fast and slow relaxation times are given by the expressions

$$\frac{1}{T_{1fast}} = 2\left(\frac{eQ}{\hbar}\right)^2 J(\omega_o) \tag{2.20}$$

$$\frac{1}{T_{1slow}} = 2\left(\frac{eQ}{\hbar}\right)^2 J(2\omega_o) \tag{2.21}$$

$$\frac{1}{T_{2fast}} = \left(\frac{eQ}{\hbar}\right)^2 [J(0) + J(\omega_o)] \tag{2.22}$$

$$\frac{1}{T_{2slow}} = \left(\frac{eQ}{\hbar}\right)^2 [J(\omega_o) + J(2\omega_o)] \tag{2.23}$$

38

where $J(\omega)$ is the Fourier transform of the correlation function which is related to the fluctuation of electric field gradients and for rotational motion is of the same form as dipolar interactions and is represented as [Berendsen et al 1973]

$$J(\omega) = \frac{(eq)^2}{20} \frac{\tau_c}{1 + (\omega\tau_c)^2}$$ (2.24)

Under extreme narrowing conditions $((\omega\tau_c)^2 \ll 1)$ as in aqueous solutions of NaCl, both T_1 and T_2 relaxation curves are described by single exponential and given as

$$\frac{1}{T_1} = \frac{1}{T_2} = \frac{1}{10}\left(\frac{e^2 q Q}{\hbar}\right)^2 \tau_c$$ (2.25)

When correlation times become long enough due to restricted nuclear motion both T_1 and T_2 relaxation curves are biexponential. The ability to resolve biexponential into two components may be limited by the low signal to noise ratio and system limitations. In this case weighted average of the relaxation times may be observed given by the expressions

$$\frac{1}{T_1} = \frac{0.2}{T_{1fast}} + \frac{0.8}{T_{1slow}}$$ (2.26)

and

$$\frac{1}{T_2} = \frac{0.6}{T_{2fast}} + \frac{0.4}{T_{2slow}}$$ (2.27)

with $T_2 < T_1$.

The above explanation is applicable for single pool of ^{23}Na nuclei under going quadrupolar relaxation. In biological systems the sodium ions are present in various pools due to presence of macromolecules, membranes etc. The ions in these different pools can relax with different time constants. When these ions exchange amoung different pools a superposition or weighted average of relaxation times from different environments is observed

may also lead to biexponential or multiexponential decay and this is explained very briefly in the next section.

2.4 Relaxation of Biological Tissues

The relaxation times in biological tissues are significantly shorter than those observed aqueous solution. The values of T_2 are also considerably smaller than T_1. Since the values of relaxation times are determined by motions, structures and interactions of molecules and ions, this altered relaxation behavior indicates that the environments of molecules and ions are significantly altered as compared to aqueous solutions.

Many constituents of tissue contain hydrophilic sites which can strongly bind water molecules. In addition many macromolecules contain charged groups such as carboxyl, sulphate etc. These charged groups can attract and possibly bind counter charged ions or groups such as Na^+, Li^+, and Cl^- [Wossener 1977]. These bound molecules are rotating less rapidly as compared to free molecules which causes an increase in their correlation times. As described in the previous section and figure 2.9, the motions at or near Larmor frequency are required for more efficient relaxation. Since the free ions have very fast correlation times and the atoms on macromolecules are rotating very slowly, the relaxation in these cases is not very efficient. On the other hand condensed ions on the macromolecule surfaces are rotating in the intermediate frequency range, thus resulting in the shortening of relaxation times. Another effect of this binding of ions with macromolecules is that they can experience cross-relaxation with the nuclei of macromolecules and therefore contribute to further shorten the relaxation times [Edzes and Samulski 1977]. If these bound molecules are in fast exchange (relative to the time frame of the relaxation process) with the molecules in the free or aqueous state, it results in an altered relaxation behavior for the bulk system.

Many macromolecules contain charged sites which result in electrostatic field gradients. Since the macromolecule tumbling rates are relatively slow these electrostatic field gradients are not averaged. This causes a decrease in relaxation times especially for quadrupolar nuclei.

Another feature affecting relaxation in biological systems is anisotropic motion due to the increased size and mass of macromolecules, especially collagen. As mentioned earlier spin-spin relaxation contain terms at high frequencies i.e ω_o and $2\omega_0$ as well as a static or zero frequency term (eq 2.17). In solutions rapid motions average out the contribution of static term to zero. However, biological structures exhibit some kind of order. this order introduces additional parameter: orientation of macromolecule axis with respect to the static field. The molecules associated or bound to these macromolecules also restricted anisotropic motions. As seen in figure 2.8 and equation 2.14 the magnetic field of dipole 'a' at the position of dipole 'b' is $B_{loc} \propto (3\cos^2\theta - 1)$. Thus the dipolar interaction between the two nuclei scales as $(3\cos^2\theta - 1)$. When $\theta = 55^\circ$ then $B_{loc} = 0$, and the dipolar interaction is reduced resulting in increase in T_2 relaxation time. This anisotropy has no significant effect on T_1 [Erickson et al 1993]. In case of quadrupolar relaxation Woessner D.E. [1991] mentioned that the mathematical terms have the same orientation dependence as dipolar relaxation.

2.5 Exchange

The ions and molecules in biological environments can exist in multiple compartments e.g. tightly bound to macromolecule, inside cells and vessels, free etc. The relaxation behavior in these environments is different. Ions exchange among these environments has a significant effect on the observable NMR relaxation times. A detailed analysis of this exchange and its effects on the relaxation times is given by Leigh [1971] and McLaughlin

[1972] in case of porton nuclei. The simple model for exchange is a two state system where the ions have a definite population fraction in each state. The average time that ions reside in each state is greater than the correlation time of ions in that state so that they have different relaxation times in each environment. The exchange between these ions is described as slow, intermediate and fast (rate of exchange between the pools is slow/fast as compared to the difference between their respective relaxation rates).

In case of slow exchange the two pools of proton ions can be considered as independent and biexponential decay is observed. This biexponential relaxation is detectable if the two relaxation rates sufficiently differ from each other and the population fraction in each pool is significant. In the limit of fast exchange the relaxation time observed is thought to be the weighted average of the relaxation times in the two environments. In case of intermediate exchange multiexponential curves may be observed.

The relaxation behavior of quadrupolar nuclei is more complex since the relaxation in each pool can be biexponential. In order to understand relaxation between quadrupolar nuclei exchanging between different pools one can look at the equations developed by Bull [1972] and Goldberg [1978].

Bull showed that relaxation in general will be sum of four exponentials if one or both sites are not under conditions of extreme narrowing. The relaxation times may however reduce to the sum of two exponentials in the limit where exchange time and relaxation times at one site are much smaller than the other site. Goldberg showed that in a system with equal populations of bound and free ions there can be three exponentials in T_2 decay curve which may reduce to two exponentials in case of fast exchange. The further pointed out that the three curves may not be differentiated experimentally. Thus even in simple two state systems the observed relaxation rates relative magnitudes are dependent on the

population fractions and the exchange rates of the ions in these pools and the relaxation characteristics within each pool.

2.6 Experimental Section

2.6.1 Experimental parameters

The parameters of interest for acquiring a spectrum are:

SW: spectral width (Hz)

SI: total number of data points transformed

DW: dwell time (sec)

ACQ: acquisition time (sec)

DE: receiver dead time (sec)

Spectral width is chosen so that it is wide enough to include all the possible frequencies generated by the sample. Once the spectral width is chosen, the digitizing rate is automatically set by the spectrometer. Nyquist theorem requires that the digitizing rate = 1/DW should be greater than twice the spectral width and is given by:

$$\frac{1}{DW} = 2\,(SW) \tag{2.28}$$

After selecting the spectral width the size of the transform determines the resolution of the spectrum because the number of data points (SI) times the dwell time is the duration of the FID observed. The resolution is given by [Fukushima & Roeder 1981]:

$$\Delta v = \frac{1}{ACQ} = \frac{1}{DW \times SI} = \frac{2\,(SW)}{SI} \tag{2.29}$$

Thus increasing the spectral width with the same number of data points decreases our ability to resolve fine lines in the spectrum.

Another parameter of interest is the receiver dead time. Since the same RF coil is used for transmitting and receiving, the receiver is turned off briefly after the excitation pulse so that the pulse does not break through into the receiving signal. The dead time is automatically set by the spectrometer and is inversely proportional to the spectral width. Therefore increasing the spectral width will decrease the dead time but also lead to pulse break through into the FID. The disadvantage of a long dead time is that if the spin-spin relaxation is fast compared to the dead time, then part of the FID is lost during the time that the receiver is off and is said to be invisible to the NMR measurement. This choice of SW and SI is a trade off between spectral resolution and dead time.

2.6.2 T_1 measurement

The most common experiment used to measure T_1 is inversion recovery pulse sequence and is given as:

$$180^o - \tau - 90^o - Acquire \tag{2.30}$$

The effect of 180° pulse is to invert the equilibrium magnetization (M_o) so that it lies along $-z$ axis. Due to spin lattice relaxation $\vec{M}$ will increase in value from $-M_o$ through zero and back to its full equilibrium value M_o. After the 180° pulse and a delay τ, the partially recovered $\vec{M}$ is rotated into the transverse plane resulting in a detectable signal which reflects the magnitude of $\vec{M}$ at time τ. After the nuclei have recovered back to equilibrium the process is repeated with different τ. Thus by varying τ we can monitor how rapidly $\vec{M}$ recovers to its equilibrium position. If we plot magnitude of $\vec{M}$ versus τ, we obtain the curve as shown in figure 2.11 which is characterized by the equation

$$M(\tau) = M_o \left(1 - 2e^{-\frac{\tau}{T_1}} \right) \tag{2.31}$$

Several data points are measured for different values of τ and T_1 is determined by fitting the data to equation above.
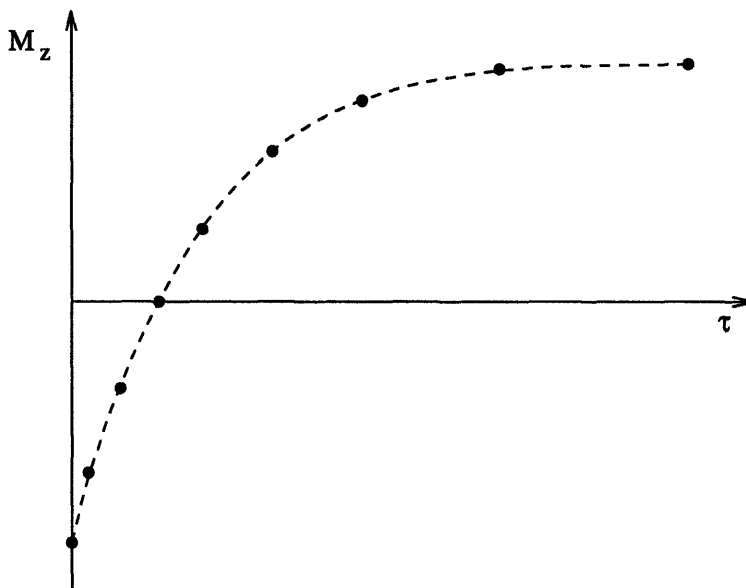
Figure 2.11: Inversion recovery measurement of T_1. The behavior of M_z for different values of τ is shown and is characterized by T_1.

2.6.3 Measurement of T_2

The rate of decay of FID is characterized by time constant T_2^* which includes the effect of static magnetic field inhomogeneities. In order to eliminate this effect and measure the intrinsic T_2 of the system a Hahn spin echo pulse sequence is used and is given as:

$$90^o - TE/2 - 180^o - TE/2 - echo \qquad (2.32)$$

The 90° pulse tips the magnetization into transverse plane. Due to magnetic field inhomogenities spins at different locations experience slightly different magnetic fields thus causing them to precess at slightly different frequencies. The effect is that spins fan out or lose coherence resulting in decreased net transverse magnetization. After time $TE/2$, a 180° pulse is applied which flips the spins into mirror images and the fast spins now lag

behind the slow ones. This causes the fast and slow spins to rephase after another time period *TE/2*.

This spin echo will compensate the static magnetic field inhomogenities but the echo amplitude also decays with increasing delay *(TE)* due to intrinsic spin-spin relaxation effects. These intrinsic spin-spin effects are irreversible and cannot be refocused. A plot of echo amplitude versus echo delay is shown in figure 2.12. This data is then curve fit to the following equation to obtain T_2:

$$M(TE) = M_o e^{-\frac{TE}{T_2}} \tag{2.33}$$

If the magnetic field inhomogenities are time variant or if the spins diffuse during the interval *TE*, the echo amplitude will decrease at a faster rate than expected from T_2 effects because these diffusion effects cannot be refocused. The effect of this diffusion is greater for longer echo delays and the echo amplitude is given as

$$M = M_o^{-\left(\frac{TE}{T_2} + \frac{\gamma^2 DG^2 TE^3}{12}\right)} \tag{2.34}$$

In order to reduce the effect of diffusion the above Hahn spin echo is modified which drastically reduces the effect of diffusion. This sequence is known as Carr-Purcell-Meiboom-Gill (CPMG) pulse sequence and is given as

$$90^o - \tau - 180^o - 2\tau - 180^o - 2\tau - 180^o \tag{2.35}$$

In this process the spins are continuously being refocused the diffusion effects can be minimized by decreasing the time interval τ that is available for the spins to diffuse before an echo is generated.
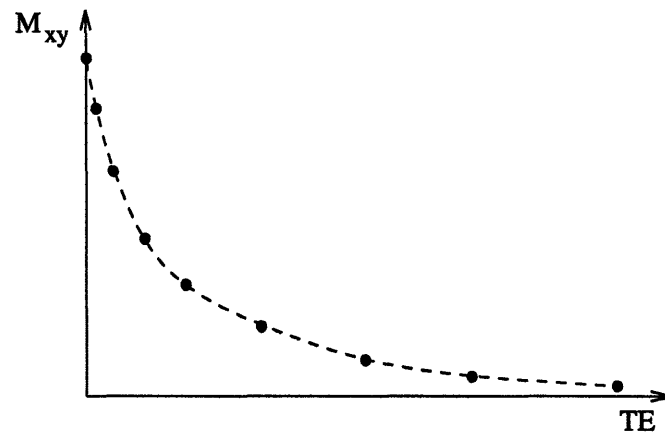
Figure 2.12: Spin-echo measurement of T_2. The behavior of M_{xy} for different values of TE is shown and is characterized by T_2

Chapter 3

Cartilage Physiology

Articular cartilage is a dense connective tissue which covers the bone surfaces of the synovial joints and acts as a load bearing material. It also provides a smooth surface for joint movement due to its low coefficient of friction. "Adult Articular Cartilage' edited by M.A.R. Freeman is an excellent source of information about cartilage and includes an extensive treatment of composition and structure of articular cartilage and its physico-chemical and mechanical properties. This chapter briefly describes the structure and composition of articular cartilage.

3.1 Cartilage Composition

Cartilage consists of a network of collagen fibers and a gel of proteoglycans and water. It contains very few cells (<10%) by volume and their main purpose is to maintain (through synthesis and degradation) the appropriate extracellular matrix composition — collagen, proteoglycans, noncollagenous proteins, and glycoproteins. It is this extracellular matrix that is responsible for the integrity of the tissue. Water consists of 65% to 80% of the cartilage wet weight. Most of the water in cartilage is freely diffusable and allows for the diffusion of solutes. Collagen consists of 50% to 60% of the cartilage dry weight, proteoglycans contribute about 30% to 35% and the rest is noncollagenous proteins and glycoproteins.

Collagen is an ordered assembly of molecules in the form of fibrils. Fibrils consist of polypeptide chains of amino acids and are approximately 300 nm long. These polypeptides are wrapped around each other in a triple helical fashion stabilized by cross-links.

The molecules are then arranged in arrays and further stabilized by intermolecular cross-links. (Figure 3.1). This crosslinked collagen network provides the shear and tensile strength of the tissue and limits the degree to which the tissue can swell. The collagen concentration varies across the cartilage thickness and is highest in superficial regions. The tensile stiffness of cartilage also decreases with depth from the articular surface correlating with the collagen content. Collagen molecules contain approximately equal number of carboxyl (COO^-) and amino (NH_3^+) groups. Most of these groups are ionized at physiological pH but these ionic groups compensate each other leaving the collagen with none or a slightly positive net charge.

Proteoglycans consist of proteins to which are attached numerous glycosaminoglycan side chains forming a brush like structure. These glycosaminoglycans are linear polymeric chains of disaccharide units. In articular cartilage there are two main types of disaccharide units, chondroitin sulfate and keratan sulfate (Figure 3.2). The chondroitin sulfate consist of repeating units of glucuronic acid and N-acetylgalactos amine and keratan sulfate consist of repeating units of galactose and N-acetylglucosamine. These units contain carboxyl or sulfate groups or both and are charged at physiological pH giving proteoglycans a net
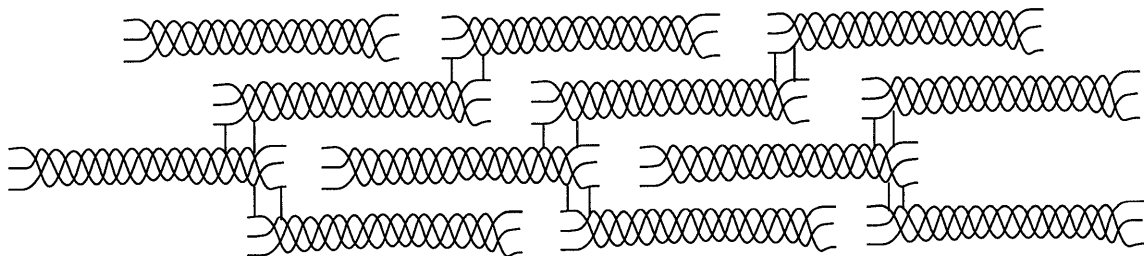
Figure 3.1: Extracellular collagen. Triple helical molecules become cross-linked and form microfibrillar bundles.

negative charge. As the charge groups are fixed to glycosaminoglycan side chains which in turn are fixed to the protein core this charge density is known as fixed charge density (FCD) and is defined as concentration of fixed groups in milliequivalents per gram of wet tissue. The proteoglycans subunits are further bound to hyaluronic acid filaments forming large aggregates. These proteoglycans, because of their negative charge and ability to interact with tissue fluid, help give cartilage resilience and stiffness to compression. If the volume of tissue decreases the glycosaminoglycan chains are pushed closer increasing resistance to further compression. The expansion of proteoglycans is restricted by the collagen network.
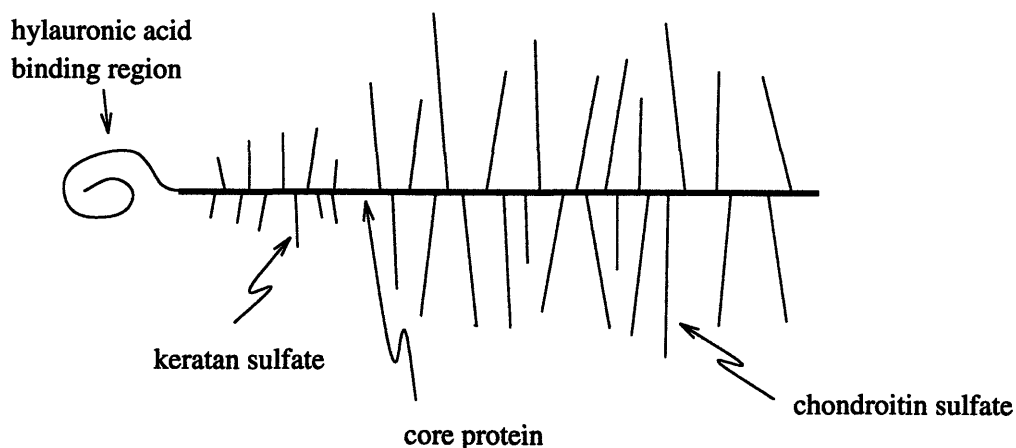
Figure 3.2: Schematic of agrecan, the predominate proteoglycan of the cartilage, showing keratan sulfate rich thin segment and chondroitin sulfate rich thick segment.

3.2 Articular Cartilage Structure

Articular cartilage composition and function varies with the depth from articular surface and has been divided into layers or zones referred to as superficial zone, transition zone, deep or radiate zone and calcified zone. Figure 3.3.

The superficial or tangential zone is adjacent to the joint cavity and occupies about 5% to 10% of total thickness. The collagen fibers in this zone are mostly aligned parallel to the surface. The cells are elongated or disc like and are arranged such that their long axis is parallel to the surface. The most superficial part of this zone is referred to as surface lamina. The water content is slightly higher in the superficial zone as compared to the other zones.

The intermediate or transitional zone occupies about 40% to 45% of total thickness. The collagen fibrils in this zone are larger than superficial zone and are more widely spaced. The fibers are mostly randomly oriented relatively to the articular surface. The cells are more spherical and evenly spaced.
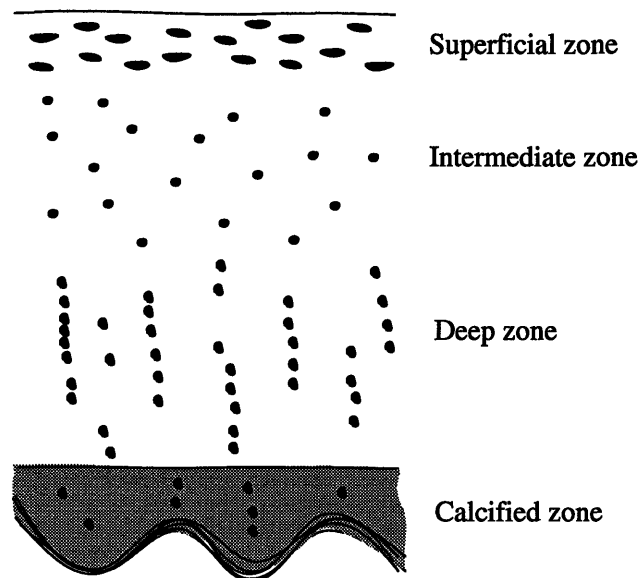
Figure 3.3: Zones of adult articular cartilage.

In the deep or radiate zone the cells are spheroidal and are arranged in columns perpendicular to articular surface. The collagen fibers are mostly oriented radial to the articular surface and form a tight mesh. This zone has the highest proteoglycan content.

Calcified zone separates the cartilage from subchondral bone and is heavily impregnated with calcium salts. The cells in this zone are slightly smaller than other zones. the collagen fibers from radial zone penetrate into the calcified zone. The deep surface of the calcified zone where it meets the bone is irregular. This zone accounts for approximately 5% to 10% of the total cartilage thickness.

3.3 Donnan Equilibrium

The presence of fixed charge inside cartilage causes an unequal distribution of mobile ions inside the tissue and in the external solution. This unequal equilibrium distribution causes a Donnan electrical potential to be set up across the bath cartilage interface. Distribution of ions obey the Donnan equilibrium equation [Maroudas A. 1979]. For cartilage equilibrated in bath of NaCl solution the concentrations of ions inside and outside the tissue obey

$$\left(\frac{\bar{\gamma}_{\pm}}{\gamma_{\pm}}\right)\left(\frac{\bar{c}_{Na^+}}{c_{Na^+}}\right) = \left(\frac{\gamma_{\pm}}{\bar{\gamma}_{\pm}}\right)\left(\frac{c_{cl^-}}{\bar{c}_{cl^-}}\right) \tag{3.1}$$

where $\bar{c}_{Na^+}$ and $\bar{c}_{cl^-}$ are concentrations of Na^+ and Cl^- in cartilage respectively

c_{Na^+} and c_{cl^-} are concentrations of Na^+ and Cl^- in external solution

$\bar{\gamma}_{\pm} = \sqrt{\bar{\gamma}_+ \bar{\gamma}_-}$ mean electrolyte activity coefficient in cartilage

$\gamma_{\pm} = \sqrt{\gamma_+ \gamma_-}$ mean electrolyte activity coefficient in solution

using ideal Donnan assumption that $\bar{\gamma}_{\pm} \cong \gamma_{\pm}$ the above equation reduces to

$$\left(\frac{\bar{c}_{Na^+}}{c_{Na^+}} \right) = \left(\frac{c_{cl^-}}{\bar{c}_{cl^-}} \right) \qquad (3.2)$$

bulk electroneutrality inside cartilage and in solution requires that

$$\bar{c}_{Na^+} + \bar{c}_{cl^-} + FCD = 0 \qquad (3.3)$$

$$c_{Na^+} + c_{cl^-} = 0 \qquad (3.4)$$

equations 3.2, 3.3, and 3.4 can be solved for FCD

$$FCD = \frac{c_{Na^+}^2}{\bar{c}_{Na^+}} - \bar{c}_{Na^+} \qquad (3.5)$$

$$FCD = \bar{c}_{cl^-} - \frac{c_{cl^-}^2}{\bar{c}_{cl^-}} \qquad (3.6)$$

therefore fixed charge density can be calculated by measuring either of intratissue sodium or chloride ion concentrations. This theory can be extended for the case of multiple ions in bath and inside cartilage [Maroudas A 1979].

Chapter 4

Previous work

In this chapter previous work on nuclear magnetic resonance techniques used to determine cartilage and joint degradation and nuclear magnetic resonance monitoring of sodium in biological tissues is presented. The first half of the chapter discusses the magnetic resonance techniques, spectroscopy and imaging, currently used to determine cartilage and joint degradation and their potential in evaluating the pathologic states. The second half briefly discusses the difficulties and issues associated with sodium nuclear magnetic resonance.

4.1 Musculoskeletal NMR

4.1.1 Knee MRI

Musculoskeletal MR imaging applications have rapidly expanded over the last several years. Earlier studies [Lai et al 1984, Reicher et al 1985a] were fairly successful in depicting the anatomical details of the knee joint. Li et al used spin echo pulse sequence and showed that MRI could delineate injuries of the menisci. Spatial resolution was limiting factor in their studies. Reicher and coworkers used a surface coil to improve the signal to noise ratio resulting in higher resolution images. They were able to differentiate between bone marrow, menisci, medial and lateral collateral ligaments. Articular cartilage was delineated as moderate intensity structure on T_1 weighted images differentiating it from adjacent low intensity cortical bone and menisci.

Reicher et al [1985b] and Burk et al [1986] used spin echo pulse sequences to study the abnormalities of menisci, articular surface, patellar tendon injuries, and cruciate ligaments. MRI findings largely agreed with arthroscopic and surgical results. In one patient

with rheumatoid arthritis several marginal erosions of the articular surface were detected by MRI that were not readily seen in radiograms. In few samples meniscal tears were seen on MR images but not on arthrograms. Yulish et al [1987] further showed that MRI could accurately depict the posterior patellar cartilage and demonstrate areas of focal swelling, surface irregularity, areas of thinning and areas of cartilage loss in case of chondromalacia patella. They also showed that T_2 weighted images were very useful for arthrogram effect of joint fluid and fluid extensions to subchondral bone through cartilage ulcers could be seen.

Mink and coworkers [1988] studied tears of cruciate ligaments and menisci of the knee in large samples (459 patients) and found the accuracy ~93%, false negative rate ~5% and false positive rate ~10%. They proposed that the false positive results could be due to intrasubtance tear and not extending to the surface. Herman and Beltman [1988] examined these false positive readings and found that most of these results were caused by low signal intensity structures like lateral inferior genicular artery, transverse ligament, popliteus tendon which are not readily observable and mimicked detachment or tear. They also showed that as menisci is curved at ends the high signal intensity artifact due to fat in the outer end due to concavity can appear within the low signal intensity fibrocartilage of meniscus. They illustrated that most of these artifacts could be removed by experience and by tracing these structures on adjacent sagittal and coronal images.

Other studies [Drape et al 1990] have used contrast agents to enhance delineation between different tissues and evaluation on abnormalities. More recently [Peterfy et al 1994] have demonstrated the use of saturation transfer and fat suppressed techniques to provide increased contrast among articular structures in arthritic knee.

4.1.2 Cartilage NMR

Due to its multiplanar imaging capabilities and soft tissue contrast NMR has proved to be well suited for diagnostic imaging of cartilage tissue. Gylys-Morin and coworkers [1987] used standard spin echo technique to study experimentally created cartilage lesions in cadaveric knees. Cartilage defects as small as 3mm in diameter were consistently observed in presence of intraarticular saline solution. With intraarticular injection of Gd-DPTA defects as small as 2mm diameter were consistently observed with reduction in total imaging time.

Adam et al [1991], Konig et al [1988] and Bongartz et al [1988] used various pulse sequences for the detection of hyaline cartilage defects of the femoral condyle, tibial plateau and hip. Common affects observed by them were narrowing in joint space, areas of increased and decreased signal intensity and complete loss of cartilage.

Chandani and coworkers [1991] used hybrid fat suppressed (HFS) spin echo technique with and without intraarticular administration of saline and gadopentetate dimeglumine in evaluation of cartilage defects in cadaveric knees. They found that T_1 weighted HFS pulse sequence provided excellent contrast between cartilage and surrounding tissues while on T_2 weighted HFS images the contrast between cartilage and saline solution was lost. In presence of intraarticular gadopentetate dimeglumine the contrast between cartilage and surrounding solution was minimal. Thus T_1 weighted HFS sequence without gadopentetate dimeglumine provided better contrast between cartilage and surrounding structure than standard spin echo in presence of intraarticular gadopentetate dimeglumine. Rechet et al [1993] reported that fat suppressed spoiled GRASS (SPGR) sequence is significantly better than standard spin echo, GRASS and non-fat suppressed SPGR sequences. The lesions were evaluated only in the presence of intraarticular saline which improved the detection of surface irregularities with fat suppressed SPGR. Thus fat suppressed

sequences have the ability to increase contrast in vivo without presence of any contrast agent and hence preserves the noninvasiveness of MR examination.

Lehner et al [1989] first studied the structure and function of bovine articular cartilage. They observed two layers of cartilage with different signal intensity patterns. On T_1 weighted inversion recovery sequence the superficial cartilaginous layer was low signal intensity and deep layer was of high signal intensity. In T_2 weighted sequence the signal intensity pattern was reversed indicating that the superficial layer had long T_1 and T_2 while deep layer had short T_1 and T_2. They attributed this difference to the variation in water content (surface layer ~84% and deep layer ~75%). They concluded that the superficial layer observed corresponded with tangential and transitional zones while deep layer corresponded to the radial zone. They also found that when the plug was subjected to static loading the superficial layer deforms and fluid shifts to the unloaded regions. With increased pressure the signal intensity in the deep layer increased in T_1 weighted inversion recovery image indicating a loss of fluid in the deep zone of loaded cartilage. Hayes and coworkers [1990] also noted that on T_1 weighted spin echo sequence the normal patellar cartilage showed either homogeneous intermediate signal intensity but more often a bilaminar appearance with low signal intensity in deep layer and high signal intensity in superficial layer was observed. They did not try to explain this effect.

Modl et al [1991] found three different zones of signal intensity in articular cartilage with long and short spin echo images and attempted to correlate these with the histologic zones of normal cartilage. Low signal intensity zone was present at the junction of cartilage and subchondral bone which the related to radial and calcified cartilage and cortical bone. A middle zone with high signal intensity was correlated to transitional zone and a low signal intensity superficial zone was correlated to compact tangentially oriented collagen fibers. The superficial zone corresponded in location but not in thickness to the

superficial zone in histologic sections. The other zones corresponded approximately to the histologic sections. They suggested that the orientation of collagen fibers may affect the signal intensity in different zones by means of its affect on magnetic susceptibility. More recently Rubenstein et al [1993] proposed that orientation dependence of T_2 due to aniso-tropic motion of water molecules parallel to the direction of collagen fibers are the cause of this effect. They showed that the alignment of cartilage specimen at different angles exhibited strong variations in signal intensities from various zones. In oblique orientations the cartilage appeared homogeneous through the three layers. The signal intensity of the middle layer changed to a greater degree than the other two with maximum signal inten-sity at oblique orientations. The superfacial layer also exhibited the same pattern as mid-dle layer but its base levels were higher than middle layer, which they attributed to greater water concentration in superficial layer. The signal intensity of lamina three remained con-stant which they speculated to be due to lack of orientation of collagen fibers as seen on transmission electron microscope.

Other studies [Paul et al 1991, Wilson et al 1993] were performed to test the potential of MRI in evaluation of cartilage composition and structure with pathologic interventions. Paul and coworkers showed that with intraarticular injection of papin (which reduces car-tilage proteoglycan content without disrupting the cartilage surface or changing the articu-lation of the joint) the cartilage thickness decreased in MR images the thickness started recovering after 72 hours papin injection. No consistent changes in proton density or T_1 and T_2 relaxation times were observed. Wilson and coworkers used interleukin-1 infusion (to initiate cartilage degradation) in rabbit knees and saw a decrease in cartilage thickness on MR images with loss of proteoglycan as seen by loss safranin-O staining in histologic studies.

Kusaka et al [1992] used MRI in conjunction with Mn^{+2} ions in saline solution. They showed that positively charged Mn^{+2} ions are good contrast agents for articular cartilage because of its interaction with negatively charged proteoglycans in cartilage matrix. Gd-DTPA was not as effective in providing good contrast. Gd-DTPA is negatively charged in contrast to Mn^{+2}. This causes repulsive force proteoglycans and Gd-DTPA. Thus the mechanism of contrast enhancement due to Mn^{+2} and Gd-DTPA is different. The disadvantage of using Mn^{+2} in vivo is that it is toxic to cells.

The above studies of looking at cartilage anatomical details to diagnose cartilage diseases do not address the issue of detection of one of the earliest changes in arthritis (a major disease of cartilage). The studies of Kusaka et al of using Mn^{+2} as a contrast agent will help determine the loss of proteoglycans from tissue but due to the toxic nature of Mn^{+2} is not suitable for in vivo studies. Lesperance and coworkers [1992] used sodium as an indicator of cartilage proteoglycan content. Because of electrostatic interactions between negatively charged glycosaminoglycans and positively charged Na^+ ions the sodium concentration varied with the proteoglycan content in the tissue. They also observed parallel changes in sodium concentration and fixed charge density when the cartilage was exposed to baths of differing salt compositions, pH or ionic strength. Sodium concentration also tracked changes in FCD when the cartilage was depleted of proteoglycans by exposure to trypsin.

Thus sodium MRI offers the possibility of detecting arthritis in its earliest stage as opposed to the above reported studies of detecting cartilage disorders which are concerned with the anatomical details. In the above studies the cartilage disorders will only become visible when gross structural changes have occured and this limits the development of preventive and curative stratagies. Once the cartilage is destroyed there is little hope of curing arthritis and the most common treatment left is pain killing and anti-inflammatory drugs.

With sodium MR images early in vivo diagnosis of arthritis is possible and may be helpful in developing therapeutic stratagies.

4.2 Sodium NMR

The study of sodium in biological systems is critical to understand physiology and pathophysiology. In order to obtain diagnostic sodium nuclear magnetic resonance images various issues should be kept in mind.

4.2.1 Spectroscopy

In earlier reports on frog muscle [Martinez et al 1969], various cell suspensions [Goldberg and Gilboa 1978] the NMR visibility of sodium concentration varied in the vicinity of 40%. The conclusion drawn by these earlier researchers was that there are two pools of sodium, bound and free, the bound fraction being invisible due to the broadening of the linewidth. Hubbard [1970] on theoretical grounds showed that even in a single pool of ions sodium may decay with two different time constants due to quadrupolar effects. 40% of the signal decays with a slow time constant and 60% of the signal decays with a fast time constant resulting in the invisible fraction. Shporer and Civian [1972] found that only 40% of the ^{23}Na was visible in sodium linoleate crystals in water. They suggested that interpretation of the earlier results should include quadrupolar effects, and that perhaps 60% of the signal was invisible due to the quadrupolar interactions rather than the splitting of sodium ions into bound and free populations. These quadrupolar effects were also observed in skeletal muscle [Chang and Wossener 1978], hydrated DNA [Berendsen and Edzes 1973]. Berendsen and Edzes 1973 developed a theory of quadrupolar effects in biological systems dependent on the structural order in systems. Goldberg and Gilboa [1978] interpreted the biological systems based on the theory of quadrupolar relaxation, rate of

chemical exchange between two sites and ratio between free and bound sodium fractions. Due to the complexity of biological systems no clear interpretation has yet been achieved.

In earlier studies total NMR visibility was determined without distinction between the intracellular and extracellular components. Most of the recent work is done to distinguish between the intracellular and extracellular components. Several paramagnetic shift reagents were used to differentiate between the extracellular and intracellular sodium compartments. These shift reagents cannot pass through cell membranes. Thus they are localized in the extracellular space and result in a shift in resonance frequency of sodium ions. Thus two different resonances are observed; one corresponding to the ions in compartments with shift reagents one corresponding to the ions in compartments without shift reagents (extracellular ions). These shift reagents have been applied to various biological tissues, red blood cells [Shinar and Novan 1984, Pettegrew et al 1984, Burstein and Fossel 1987a, Shinar and Novan 1991], perfused hearts [Burstein and Fossel 1987b, Pike et al 1985, Foy and Burstein 1992], dog brain [Eleff et al 1993] to study intracellular sodium concentration, and transport of ions across cell membranes. In recent reports using shift reagents full NMR visibility of sodium has been reported in erythrocytes [Pettegrew et al 1984] but conflicting studies [Nissen et al 1989] report that part of sodium (~30%) is still invisible. Differences in equipments and experimental techniques may be responsible for these variations.

Practically always less than 100% of sodium is visible and is variable from tissue to tissue. Variations in cell environments within tissue create different compartments which may alter sodium relaxation parameters (hence its NMR visibility). In order to obtain quantitative tissue sodium concentrations the percentage of sodium invisible to NMR should be carefully determined.

4.2.2 Sodium Relaxation Times

In standard NaCl solutions at 25°C both T_1 and T_2 values were found to be 59ms, but increased to 69ms at 37°C [Burstein and Fossel 1987a] and agreed with other reported results. Shporer and Civan [1974] measured the relaxation times characterizing sodium within frog striated muscle. They found that the longitudinal relaxation time, T_1 was approximately 24ms at 23°C while T_2 consisted of both slow and fast components. The T_2 fast component was ~3ms but they mentioned that the precision of their measurement was inadequate to provide more than a rough estimate. The slow component was measured to around 14ms. They interpreted the results based on a conservative estimate of quadrupolar coupling constant and a simple model consisting of two fractions of ions, free and bound, in chemical exchange. They concluded that less than 1% of sodium is bound and it is in fast exchange with the free fraction. Monoi [1976] analyzed their data based on a more complex model with two pools of sodium. The ions in one pool consisted of a single T_1 and a single T_2 in intermediate exchange with sodium ions of the other pool where they had two different T_2's but single T_1. Their calculations showed that correlation times for sodium was in the neighborhood of 8ns which was approximately ten times smaller than that found by Shporer and Civan but they also concluded that the bound fraction of sodium was close to 1%.

Monoi and Uedira [1980] found that sodium T_1 and T_2 in dilute transparent micellar solutions exhibited a single exponential decay but in turbid emulsions and gels T_2 showed biexponential relaxation. They further found that the occurrence of two T_2 values correlated with the dimensions of colloidal particles and the only requirement for two T_2 values is that colloidal particles should not be less than 30 or 40nm. They also found that when nonionic groups were substituted for the carboxyl group on fatty acids even the presence of large emulsion particles did not produce two different T_2 values. They explained the

relaxation behavior by two pools, a bulk aqueous phase characterized by fast tumbling in exchange with the sodium ions on the surface of colloidal particles that were undergoing quadrupolar relaxation such that two different T_2 values occurred and ionic groups on those colloidal particles particles were necessary to produce the biexponential decay.

Several other studies were also conducted in the mean time about the interaction of sodium with biological tissues and attempts were made to estimate the correlation times using different models. Bull et al [1972] studied T_1 and T_2 relaxation times of ^7Li, ^{23}Na, and ^{35}Cl ions in absence and presence of oxy- and carbon monoxyhaemoglobin to determine the interaction of ions with macromolecules. They found that ^{35}Cl and ^7Li strongly interact but sodium did not interact for concentrations up to 0.5M. Lerner and Torchia [1986] also did not find any evidence of sodium ions binding to solutions of proteoglycans and the correlation times were always in the extreme narrowing region because T_1 was equal to T_2. They also observed that sodium relaxation rates increased by increasing the concentration of proteoglycans in solution. Chang and Wossener [1978] found that in rat skeletal muscle sodium can be modeled as being distributed as a single compartment associated with macromolecule charged sites undergoing quadrupolar relaxation and the autocorrelation function consisted of the sum of two different correlation times giving them an upper and lower bound on correlation times.

Sodium relaxation times were measured in human blood, erythrocytes and plasma [Pettegrew et al 1984]. T_1 and T_2 were both found to be monoexponential with T_2 less than T_1 indicating that extreme narrowing condition does not apply and there is a lengthening of correlation time. In a parallel study the relaxation times of human and dog erythrocytes were measured by Shinar and Navon [1984]. They also found that T_1 and T_2 are monoexponential with values 20.7ms and 11.3ms respectively. These intracellular relaxation times did not vary the concentration of shift reagents or intracellular sodium. With a

better spectrometer capable of recording short echo times they were able to resolve the T_2 relaxation time into two components and concluded that the monoexponential T_2 can be considered as weighted average of the two components. They found that very little sodium was bound to hemoglobin. The transverse magnetization in suspensions of chicken erythrocytes was found to decay biexponentially [Shrinar and Navon 1991] and were considerably shorter than those in human and dog erthyrocytes [Shrinar and Navon 1984]. The short component of T_2 which is more sensitive to the binding to macromolecules showed a two fold decrease as compared to mammalian erythrocytes. The major difference between chicken and mammalian erythrocytes is the presence of nuclei in chicken erythrocytes. Transverse relaxation times found for suspensions of nuclei was also biexponential and removal of nuclear membrane had no significant effect on the relaxation times. The relaxation times also did not depend on intracellular sodium concentrations consistent with the previous studies on human and dog erythrocytes.

Intracellular sodium T_1 values for perfused rat hearts were found to be around 25ms. For perfused rat hearts intracellular sodium relaxation times were determined by Burstein and Fossel [1987b] using the shift reagent dysprosium tripolyphosphate $Dy(PPP)_2^{7-}$. They also presaturated the extracellular sodium signal so as to minimize its contamination of the intracellular signal. They found that intracellular T_1 was 23ms and T_2 had two components, 2ms and 16ms, with relative amplitudes of 0.47 and 0.53 respectively. Based on these observations they postulated that approximately 80% of the intracellular sodium is in one homogeneous pool with T_2 values of 2ms and 16ms for fast and slow components respectively and an average T_1 of 23ms. The rest of the sodium is in a separate pool with fairly short correlation time such that T_1 is approximately equal to T_2 which is between 20-25ms. They mentioned that other models for fitting the relaxation time data are also possible given the number of variables in biological systems. Addition of ouabain in their

study produced a five fold increase in sodium concentration over control levels but this increase had a negligible effect on sodium relaxation times. This is consistent with the studies reported by Shinar and Navon on red blood cells. They proposed that the increase in sodium concentration is displaced by intracellular potassium at the binding sites and an increase in concentration may be accompanied by increase in sodium occupancy of binding sites such that the percentage of sodium ions which are bound remains constant.

Extracellular sodium in perfused rat hearts [Foy and Burstein 1992] also showed biexponential T_2 decay with fast and slow components of 2.1ms and 26.3ms respectively. With pathologic interventions of ischemia and extracellular edema the magnitude of sodium increased to 300% and 500% of control values respectively but the T_2 decay did not show any trends with these pathologic interventions. This and the previous studies about intracellular and extracellular relaxation rates showed that relaxation times for both intracellular and extracellular sodium ions exhibit quadrupolar interactions and the transverse relaxation component may exhibit multiexponential characteristics.

4.2.3 Sodium Imaging

The characteristic of sodium magnetic resonance imaging in biological systems different from proton imaging is the presence of very short T_1 and T_2 relaxation times for sodium. Short T_1 relaxation times are advantageous because short recycle delays (TR) can be used which reduces total imaging time when multiple scans are acquired for signal averaging. Due to its fast T_2 decay and low concentration of sodium in tissues the major effort of the researchers was to design pulse sequences for sodium imaging so that images at shortest possible echo times can be achieved. This is necessary order to preserve as much of sodium signal as possible during the echo delay. The first part of this section describes the techniques developed by researchers to obtain short echo times the second

part examines the feasibility of sodium imaging in determining the distribution and properties of sodium in tissues and its potential use in distinguishing between healthy and diseased tissue.

The first sodium images of a biological system were produced by Delayre et al [1981]. They used a projection reconstruction technique to produce images of isolated perfused rat heart. The projection reconstruction technique was used because it produces images from the free induction decay (FID) signal instead of the spin echo signal to minimize the loss of the short T_2 fraction of sodium. They were able to clearly differentiate the signal from perfusate and healthy tissue. By gating the NMR imaging process to cardiac cycle they also demonstrated an increase in wall thickness in systole and an increase in cross-sectional area of the ventricular cavity in diastole.

In vivo images of heart, kidney and brain [Ra et al 1988, Ra et al 1989] were obtained by using three dimensional planar integral projection reconstruction methods where all three gradients are used for readout to provide projection data. They also extended their pulse sequence to include multiple spin echo images at echo times of 18ms and 36ms to provide information about the long T_2 decay of sodium. Blood with long T_2 gave strong signal for both projection image and spin-echo image. By subtraction of the FID image and the spin-echo image with T_2 compensation, the short T_2 component in the heart wall was observed. In spite of the fact that projection FID is equivalent to only half an echo, SNR in the FID image was better than that of 18ms spin-echo image because of large contribution from the short T_2 fraction.

The difficulties associated with the projection reconstruction method is that it is more sensitive to magnetic field inhomogeneity and object magnetic susceptibility effects as compared to the spin-echo technique. The rise time of gradient waveforms and their shapes can cause nonlinear effects and image artifacts.

Granot et al [1986] used a three dimensional gradient echo technique using Fourier phase encoding to produce images of the head. The elimination of 180° refocusing pulse in the gradient echo technique reduces the echo time for imaging and also reduces power deposition in the sample especially in multiple echo acquisitions. The multiple echos were acquired for signal averaging and to enhance T_2 contrast. They used spatially nonselective RF pulses to further shorten echo times. The intensity of gradient echo image decays with T_2^* but by careful shimming they were able to achieve field inhomogeniety of less than 1ppm over the entire head.

Perman et al [1986] used a three dimensional multiple spin echo technique to investigate the contrast sensitivity of sodium as a function of imaging time, spatial resolution and coil design. To reduce the echo time they used nonselective refocusing pulse and the shortest echo time achieved by them was 13ms. They found that the extracellular spaces represented by edema, vitreous humor, CSF, and physiological saline have almost identical relaxation times. Although they found that tumor had slightly smaller T_2 the difference was not enough to differentiate between healthy and abnormal tissue and were unable to differentiate tumor from bordering CSF space. They proposed that this was due to the fact that at echo time of 13ms only 14% of the fast sodium component was visible. In order to further reduce the echo time they used nonselective 90° and 180° RF pulses and used presaturating pulses to eliminate the signal from outside the desired region and were able to achieve echo times of 2.5ms [Perman et al 1989]. They were able to quantify the in vivo T_2 relaxation times for gray matter and white matter (17.6ms), vitreous humor (56.8ms), and rabbit carcinomas (T_{2f} = 3.3ms and T_{2s} = 22ms) which agreed well with the results obtained from excised tissue.

Kundel et al [1988] used a combined pulse sequence to obtain images of rat lung using both gradient echo (TE = 3.3ms) and spin echos (TE = 15.4, 28.7, 44.5, 57.9ms) in order

to obtain both short echo times reduced magnetic field inhomogenities. They found that the concentration of sodium correlated with lung water content but did not correlate with the blood content. They did not find any changes in T_2 due to changes in lung water content.

Various researchers have shown the feasibility of sodium imaging in differentiating between diseased and healthy tissues, and to calculate the differences between the concentrations of sodium in different tissue compartments. The cerebral sodium distribution in brain and in patients with a variety of pathological conditions was successfully demonstrated [Hilal et al 1985]. As compared to proton sodium showed a greater variation from normal to pathological conditions and changes in signal intensity from 200% to 500% were observed. Schuierer et all [1991] examined variety of supratentorial lesions at 4T. All those lesions were also visible on proton images and sodium images did not add any new information. They acknowledged that the TE for their experiments was 11ms and with reduced echo times the short T_2 component might make the sodium MRI more useful.

Other imaging studies were done to obtain the compartmental information about signal from the intracellular and extracellular spaces. Burstein and Mattingly [1988] used a shift reagent to produce a chemical shift difference between the intracellular and extracellular sodium. Using frequency selective pulses they were able to produce separate images of the different sodium pools.

Summers et al [1988] used dextran magnetite as a contrast agent for sodium imaging. Dextran magnetite is a paramagnetic compound which produces large local magnetic field inhomogeneities causing a reduction in relaxation times of sodium. Due to its large size it remains in extracellular space and does not effect the intracellular ions. Sodium images using contrast agent showed a significant decrease in signal intensity in liver, heart and

kidneys. They also proposed the use of this contrast agent as means of distinguishing intracellular and extracellular sodium pools instead of toxic shift reagents.

4.2.4 Multiple Quantum Spectroscopy

Sodium nuclei undergoing electrical quadrupolar interactions exhibit a biexponential decay. Sodium in heterogeneous systems exchanges between free and bound sites and also relaxes as a sum of two or more relaxation times. Pekar and Leigh [1986] used a pulse sequence that passes the spins through a double quantum filter and places the two relaxation components in opposite phase with each othersuch that the signal observed is the difference between the two components. Only nuclei with correlation times long enough to lead to biexponential decay are visible by this method. Ions under extreme narrowing conditions are not detectable by this technique and initially it was proposed by Pekar that double quantum spectroscopy can be used as an alternative to shift reagents to distinguish between intracellular and extracellular sodium components.

In dog erythrocytes they compared sodium signal from both intracellular and extracellular compartments using shift reagents and compared it to the double quantum filtered signal that contained only the intracellular signal and they concluded that DQF detects only intracellular sodium. Jelicks and Gupta [1989] showed using shift reagents and the double quantum technique that a significant contribution to the double quantum signal came from extracellular sodium. They also showed that shift reagents can quench the extracellular signal in case of erythrocytes. Therefore no signal was observed by Pekar and Leigh from the extracellular pool of sodium.

Eliav and Navon [1994] detected anisotropic motions of sodium ions in cartilage tissue using double quantum filtered techniques. DQF experiments on suspensions of collagen fibers showed similar anisotropic effects but chondroitin sulphate solutions did not

show any DQF spectra indicating that the binding of sodium and its anisotropic motion are associated with helical structures of collagen fibers.

The difficulties associated with this technique are the loss of sensitivity and the difficulty in quantifying the relaxation parameters as only the difference between the two resonances obtained.

To summarize, sodium MR imaging may have a definitive advantage in detecting arthritis at an early stage over proton MRI. The difficulties associated with sodium MRI are its short relaxation times and low signal to noise ratio. Very short transverse relaxation times require the development of short echo time imaging pulse sequences so that the sodium signal is not lost during the echo time. Also in order to obtain quantitative tissue sodium concentration maps one should be aware of the tissue sodium relaxation times and variations in these relaxation times with disease states.

Chapter 5

Methods

Interstitial sodium relaxation times were studied with spectroscopic methods for both control conditions and pathologic conditions of cartilage degradation. Described below are the sample preparation techniques including methods for inducing pathologic conditions, experimental procedures and, data analysis techniques.

5.1 Physiological Preparations

5.1.1 Epiphyseal Cartilage Explant

Bovine epiphyseal cartilage was obtained from the distal ulnas of newborn calves. Intact foreleg joints of 1-2 week old calves were obtained immediately after slaughter. The distal ulnas were exposed by cutting away all surrounding muscle and connective tissue. The ulnar periosteum was peeled off carefully so as not to damage the epiphyseal cartilage. Once the periosteum was removed the ulna was separated from radius and broken at metaphyseal/epiphyseal cartilage interface. The epiphyseal cartilage attached with bony epiphysis was placed in buffered saline solution to prevent dehydration before slicing.

The epiphysis was then fixed in a sledge microtome, after sectioning off 0.5–1 mm to remove the growth plate. Sequential 2 mm slices of epiphyseal cartilage (non-growth plate) were sectioned. The slice number one was closest to the growth plate on the metaphysis side. From each slice, 8 mm diameter cylindrical disks were cored using a dermal punch. The principal steps of cartilage explant procedure are shown in Figure 5.1. For one set of experiments 4 mm square pieces and also 4 mm diameter spherical samples of cartilage carefully sliced by scalpel were also obtained.

Microtome
Blade

Metaphysis

Epiphyseal
Cartilage

Microtome
Holder

2 mm

Epiphysis

Articular Surface

Cartilage Disks
8 mm diameter

Dermal
Punch

Bovine Distal Ulna
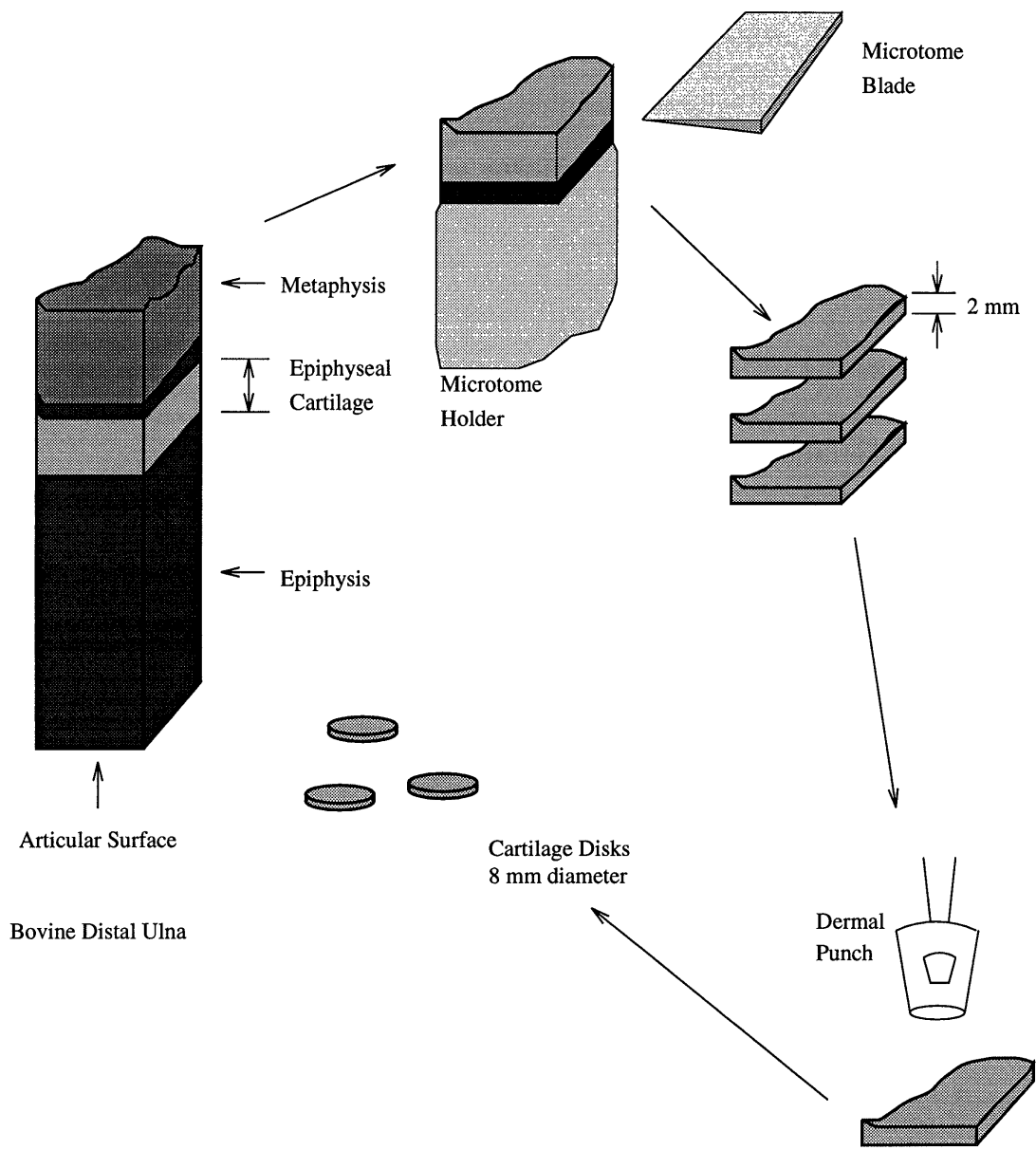
Figure 5.1: Epiphyseal Cartilage Explant

5.1.2 Articular Cartilage Explant

Knee joints from 1-2 week old calves were obtained. The femoropatellar joint was isolated by dissection of the tibia and femur. The joint capsule was then exposed by cutting off ligaments and removal of the patella and tibia. The distal segment of the femur was then mechanically supported by attachment to the mounting section of the drilling apparatus. Three to five cylindrical cores of cartilage and bone were drilled out from each section (lateral and medial) of each joint using a 9 mm drill punch. The cores were labelled from posterior end. After explant the cores were sliced and punched to obtain 2 mm thick and 8 mm diameter cylindrical disks.

5.2 Sample Preparation

Initial experiments were done on fresh and unfrozen cultured tissue samples of epiphyseal cartilage. The cultured disks after explant were kept in Dulbecco's Modified Eagles Medium (DMEM) for 11 days. DMEM was supplemented with proline (0.4mM) and non-essential amino acids (0.1mM), 20μg/ml of L-ascorbic acid and 1% fetal bovine serum (FBS). During culture the cartilage was kept in an incubator at 37 $^{\circ}$C with 5% CO_2 in air atmosphere. Preliminary results of T_2 measurements indicated that the respective T_2 parameters for pre and post freezing case were within 5% of each other for one control and one interleukin-1β treated sample. After it was determined that freezing had no effect on the NMR spectroscopy measurements the requirement for analyzing fresh or cultured tissue was relaxed and the cartilage disks were immediately frozen after explant to be used for experiments later.

Before an experiment the frozen samples were thawed and equilibrated at room temperature in 150 mM NaCl solution buffered with 1 mM Tris/Tris Hydrochloride solution at pH 8. Baths contained at least 20 ml saline per disk which is greater than 100 times the

volume of the samples. The disks were equilibrated for at least 90 minutes. This equilibration time was based on the estimates of diffusion distances for sodium: $x = \sqrt{2D\Delta}$, where x is the root mean square diffusion distance, Δ is the equilibration time and D $(0.77 \times 10^{-5}$ $cm^2/s)$ is diffusivity of Na in free swelling cartilage samples [Burstein et al 1993]. Therefore the distance travelled by the ions is approximately 0.3 cm in 90 minutes which is enough for complete equilibration of the samples used. After equilibration the disks were blotted dry to remove excess water. The wet weight of the disks was measured and then they were placed in a 10 mm capped NMR tube for the experiments.

5.3 Pathologic Interventions

We were interested in determining how sodium NMR relaxation times are affected in pathology. Two interventions which degrade the samples and mimic tissue pathology were performed.

5.3.1 Trypsin

Trypsin degrades the cartilage which leads to the loss of noncollagenous proteins and proteoglycans from the extracellular matrix of the cartilage leaving behind relatively pure collagen matrix. It also may degrade any damaged collagen. Cartilage water content is also affected by removal of proteoglycans because the removal of fixed charge density would result in decreased swelling pressure. Although total water content decreases the fractional tissue water fraction expressed as water weight over tissue wet weight may increase due to loss of solid matrix. Cartilage disks were bathed overnight in 5 ml saline containing 25 mg/ml trypsin (lyophilized porcine, from Gibco Laboratories). Cartilage was then removed from trypsin and bathed in 5 ml of fetal calf serum for approximately two hours to stop any further degradation by trypsin. The samples were then further equil-

ibrated in fresh saline bath for at least 90 minutes before being used in an NMR experiment.

5.3.2 Interleukin-1β

Interleukin-1β bioactivity has been identified in the synovial fluid of patients suffering from joint diseases and these activities have been clearly correlated with the activation of metalloproteinases and proteoglycanases which degrade extracellular matrix in arthritic conditions [Dayer et al 1979, Henderson et al 1990]. Treatment of viable cartilage with IL-1β results in a progressive dose dependent release of tissue proteoglycans. Freshly harvested epiphyseal cartilage samples were cultured in Dulbecco's Modified Eagle's Medium containing IL-1β. The cartilage was kept in organ culture throughout the experiment because effectiveness of IL-1β requires viable cells. 1% fetal bovine serum was added to the culture media to feed the cells. At the end of the culturing period (11 days) tissue wet weights were taken and then the samples were used for spectroscopy experiments.

5.4 NMR Methods

NMR spectroscopy experiments were performed on 8.45 Tesla Bruker spectrometer (Bruker Instruments, Inc. Billerica, MA) operating at 360 MHz for protons and 95.26 Mhz for sodium. A standard broad band probe was used for all experiments. All experiments were performed at room temperature.

5.4.1 One Pulse

Sodium and proton spectra were obtained with a standard 90° pulse sequence. The 90° pulse lengths for typical samples in broad band probe were about 15 μsec for sodium, corresponding to 10 mm sodium coil and 30 μsec for protons corresponding to 15 mm proton

coil. Recycle delay of $5T_1$ (3 ms for sodium and 20 ms for protons) was used between successive excitations to ensure complete relaxation of nuclei. Unless otherwise stated a, spectral width of 10 kHz with a spectrometer delay time (DE) of 65 μsec was used. Typically 2000 or 4000 scans were collected for sodium to improve the FID signal to noise ratio resulting in total data collection time of 20 min. Time domain data were processed using complex Fourier Transformation (FT) and the resulting spectra were integrated to obtain area under the spectrum. The area under the resonance curve is proportional to the number of nuclei present in the sample. By calibrating these signals to those obtained using standards with approximately the same volume as the cartilage plugs (100 μl of 150 mM NaCl solution for these experiments) the water or sodium content in the cartilage plugs under study was determined. Previous studies have shown that there exists a linear relationship between the NMR signal and tissue ion content [Lesperance et al 1992].

5.4.2 Sodium Concentration Calculations

In order to determine sodium concentration in the cartilage plugs from sodium content as determined by NMR the water content is required. Sodium content was converted to intratissue ion concentration by normalizing with water content. After the experiments the cartilage disks were lyophilized to determine the dry weights and the water content was calculated by difference between wet weights and dry weights (assuming 1 gm = 1 ml) and compared to that found by NMR.

The sodium ion concentration was determined as follows

$$Na = \frac{concentration\ of\ standard \times volume\ of\ standard \times area\ under\ spectrum\ of\ cartilage}{area\ under\ spectrum\ of\ standard \times water\ content} \tag{5.1}$$

5.4.3 Fixed charge density (FCD) calculations

Fixed charge density was calculated from intratissue ion concentration as measured by NMR using ideal Donnan theory (Section 3.3) and is given by the equation

$$FCD = \frac{[Na^+]_b^2}{[Na^+]_t} - [Na^+]_t \tag{5.2}$$

5.5 Relaxation time measurements

Sodium relaxation times measured in the following sections are for cartilage orientation with the longitudinal axis (epiphysis to metaphysis for EP cartilage and perpendicular to the articular surface for AC cartilage plugs) parallel to the magnetic field.

5.5.1 T_1 measurements — Inversion recovery

Sodium spin-lattice relaxation times (T_1) were measured for saline and cartilage. T_1 values were obtained by inversion recovery pulse sequence (Section 2.6.2). Inversion delays were varied from 1 ms to 150 ms. A total of twelve data points were collected with 1000 averages, resulting in a total collection time of 45 minutes.

The T_1 data was fit to a single exponential, equation 5.3, with a least square curve fitting program implemented on IBM PC

$$M_z(t) = M_o\left(1 - 2Ae^{-\frac{t}{T_1}}\right) \tag{5.3}$$

where A in the above equation compensates for any error in finding and using the exact 180° pulse in the experiment.

5.5.2 T_2 measurements — Hahn echo

For sodium spin-spin relaxation time measurements a Hahn spin echo pulse sequence (section 2.6.3) was used and 19 to 26 data points consisting of echo times ranging from 10 μsec to 30 msec were collected. The spectral width of 10 kHz was used which contributed an additional equipment dead time of 65 μsec to the echo delays. Due to the limitations on the power output of the spectrometer, which limited the 180 $^\circ$ pulses to be transmitted at intervals greater than 2 ms, the CPMG pulse sequence could not be used to measure the fast T_2 decay of Na in tissue.

Because of very low signal to noise of sodium, long acquisitions (2000 or 4000 excitations) were collected for each data point to obtain reasonable signal to noise levels. For some cases the data points with long echo delays were run separately to allow for increased signal averaging. One data point was overlapped for the two half of the lists so as to determine any systematic error in running the two halves separately. The entire T_2 experiment took about one and a half to two hours. In order to compensate for possible changes over time the echo delay list was modified. The list was written such that first half of the list contained delays in descending order, the rest of the list contained delays interleaved between the first half. Any changes over time by this arrangement of delay list would be evident with all alternate points being consistently high or low. From T_2 data it was obvious that a single exponential fit was not enough therefore double exponential fit was performed, characterized by the equation

$$M(t) = M_f e^{-\frac{t}{T_{2f}}} + M_s e^{-\frac{t}{T_{2s}}} \tag{5.4}$$

where M represents the magnitude of the signal acquired as a function of time, T_{2f} repre-

sents the fast component of spin-spin relaxation time with magnitude M_f, T_{2s} represents the slow time constant with magnitude M_s. Less than two time constants did not provide a good fit, and more time constants were not justified for the available signal to noise ratio and the number of data points acquired.

Note that the double exponential merely provides a characterization of the data obtained in sodium relaxation experiment and not a description of time constants which may be physically present.

Since relaxation times are generally found to increase with increased water content in the tissues [Crooks et al 1987], the cartilage disks were also consistently weighed before and after the experiment and percentage loss in weight was determined. This loss in weight was less than 3% for the entire course of the experiment. This confirmed that loss of water from the disks was presumably not significant enough during the course of experiment to affect the relaxation times.

5.5.3 T_{2fast} by varying the dead time

From a practical standpoint it is advantageous to decrease the dead time of the equipment so that the signal decay during this dead time could be kept to a minimum. One problems associated with a short dead time is that it may not be enough for the excitation pulse to decay to zero and the resulting signal will be sum of the true signal from tissue and a part of the excitation pulse. For this study we were interested in characterizing the relaxation times, therefore to back up our estimates of T_{2f} as determined by Hahn echo we varied the dead time of the instrument to determine the fast relaxation component as described below.

Spectral width (SW) was adjusted to decrease the dead time (DE) of the spectrometer. The dead time for this spectrometer is calculated by the equation 5.5 where dwell time (DW) is equal to 1/2(SW)

$$DE \text{ (sec)} = 1.25 \times DW + 2.5 \times 10^{-6} \qquad (5.5)$$

One pulse experiments were performed with large data averages and spectra were collected for spectral widths of 10 KHz, 20 KHz, 30KHz and 50 KHz corresponding to dead times of 65 μs, 33 μs, 22 μs and 15 μs respectively.

The spectra were carefully integrated and T_{2f} was determined by using least square curve fitting procedure according to equation 5.6 (At these small times the signal decay due to the slow component is less than 1%).

$$ln(M) = -\frac{DE}{T_{2f}} + ln(c) \qquad (5.6)$$

5.5.4 T_{2fast} from Linewidths

Quantitation of the fast T_{2f} decay is important because changes in it are likely to affect the signal intensity in MR images for short echo times. In order to determine how well the linewidth reflected the actual T_{2f} of the system as determined by the Hahn spin echo sequence one pulse experiments were run with large signal averages. When the spectrum obtained had a well defined broad component as shown in Figure 5.2, the linewidth at the half height of the broad component was carefully determined by eye and T_{2f} was calculated by equation 5.7 and compared to that determined by Hahn echo sequence.

$$T_2 = \frac{1}{\pi \upsilon_{1/2}} \qquad (5.7)$$
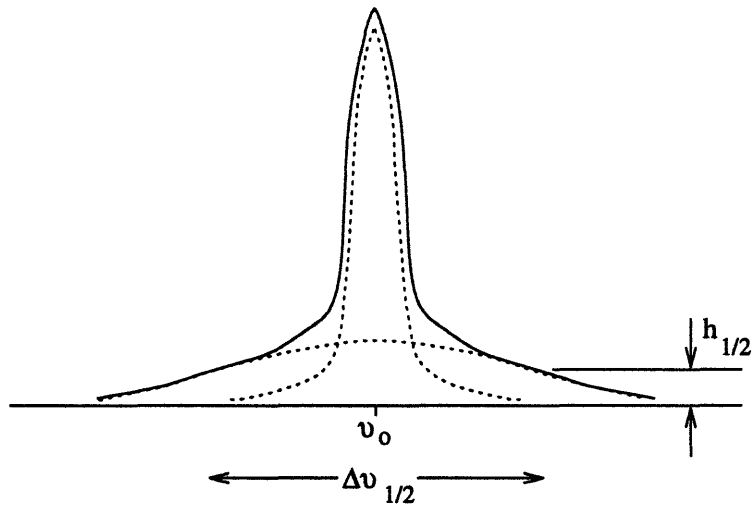
Figure 5.2: NMR spectrum of Na in cartilage. The linewidth ($\Delta v_{1/2}$) corresponding to half height of the broad component was determined.

5.6 Desorption Studies

Studies were done to determine if sodium ions in cartilage are totally visible by NMR at receiver dead time of 65 μsec. Cartilage plugs were put in solution so that sodium in tissue would desorb in the solution. Measurements were done to determine if the ion content desorbed in the solution was equivalent to or greater than that measured in the tissue. All ions are visible in the solution because the T_2 values in the solution are long relative to the receiver dead time.

Ions in the tissue may be invisible due to the short T_2 values compared to the receiver dead time. The measured T_2 values from Hahn spin echo experiments were used in equation 5.4 to determine what fraction of ions is invisible at delay time of 65 μsec and compared to the desorption studies. This was done to determine if the mesured T_2 would represent all of the mobile sodium in the tissue.

Sodium concentration in cartilage disks was measured by NMR with a receiver dead time of 65 μs. 150 mM KCl solution was then added to the cartilage plugs in the NMR

tubes so that intratissue sodium would diffuse out of the tissue. Large desorbing volumes are more effective for desorption of sodium but this would result in having solutions outside the sensitive regions of the NMR coil. Therefore desorbing volumes were selected such that the ratio of tissue water to the added KCl solution was 1:10 and the volumes remained in the sensitive regions of the coil. After 5 hours the sodium content in the cartilage/KCl ensemble was again measured. One thing should be kept in mind that if the invisible sodium does not desorb it would still remain invisible. The cartilage was then removed from the solution, blotted dry and was tested by NMR for remaining intratissue sodium content. The data were analyzed to determine the invisibility fraction of sodium in cartilage.

5.7 T_2 dependence on orientation

In biological tissues, the increasing size and mass of macromolecular structures cause anisotropic motion to become an additional factor of importance in NMR relaxation. Collagen containing tissues are more prone to this effect [Erickson et al 1993, Peto et al 1990].

5.7.1 T_2 at two perpendicular orientations

To establish whether relaxation measurements depended on tissue orientation square cartilage samples were held in the NMR tube in two different orientations and two different sets of data were collected. In the first set the cartilage samples were placed in the NMR tube such that metaphysis to epiphysis axis was held parallel to the direction of the magnetic field B_0. For the second set the cartilage was held perpendicular to the first orientation i.e the metaphysis/epiphysis axis was now perpendicular to magnetic field (Figure 5.3).

One possible source of error that could cause differences in the relaxation time measurements is the magnetic susceptibility effects due to the geometrical shape of the cartilage plugs. To remove this bias spherical samples were used in the following experiment.

5.7.2 T_2 vs. orientation angle

To determine the variation of T_2 at different angles teflon spacers were made such that their top surface was sliced at increasing 10° angles. A spherical piece of cartilage was used for this experiment and it was glued to the top of the spacers using a small drop of Vet Bond (3M - St-Paul, MN) tissue adhesive. Tissue adhesive tested alone did not give any NMR signal. The cartilage was held such that the metaphysis to epiphysis axis as shown in Figure 5.4 made an angle θ with the static magnetic field. The angle θ was varied from 0° to 90° in increments of 10° and T_2 was determined for each orientation.The cartilage was returned to NaCl bath for equilibration in between each increment of the angle. Because of the time requirements it takes to determine T_2 only one sample was used in this experiment.

E: epiphysis
M: metaphysis
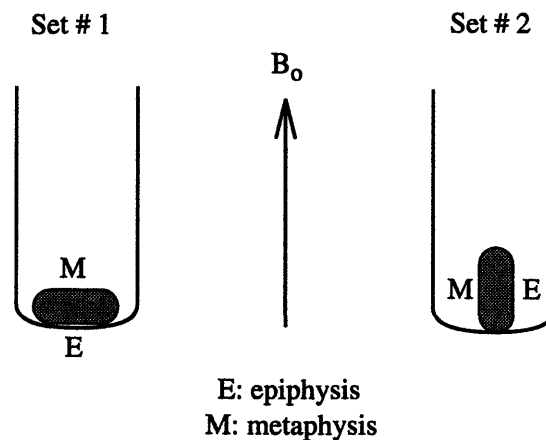
Figure 5.3: Cartilage orientation
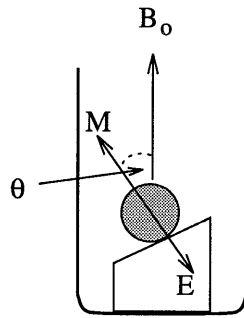
E: epiphysis
M: metaphysis

Figure 5.4: T_2 dependence on orientation

5.8 Implication for MR Imaging

As described previously MR images are weighted by two experimental parameters, repetitition time (TR) and echo delay (TE), and three tissue parameters, density of sodium ions (N), and the two relaxation times T_1 and T_2. For a given choice of experimental parameters any changes in the relaxation times can cause an error in our ability to quantify the tissue sodium concentration. It is not possible to determine sodium relaxation times every time with imaging. Therefore with the determined worst case variations in relaxation times the error in quantifying sodium concentration was calculated with resonably feasible imaging parameters.

For the case when the transverse relaxation (T_2) has a single exponential decay the signal intensity is given by:

$$ S = N\left(1 - e^{-\frac{TR}{T_1}}\right)\left(e^{-\frac{TE}{T_2}}\right) \tag{5.8} $$

When the transverse relaxation is biexponential, which is usually the case for sodium ions in biologically tissues and also for our case, the equation for signal intensity is modified slightly and is given as

$$S = N\left(1 - e^{-\frac{TR}{T_1}}\right)\left(S_f e^{-\frac{TE}{T_{2f}}} + S_s e^{-\frac{TE}{T_{2s}}}\right) \qquad (5.9)$$

where T_{2f} and T_{2s} are the fast and slow relaxing components and S_f and S_s are the respective fractions with which the fast and slow components relax.

5.8.1 Correction for variations in T_1

To determine errors caused by saturation due to the fast repetition times we used TE = 0 ms in equation 5.9 which then reduces to

$$S = N\left(1 - e^{-\frac{TR}{T_1}}\right) \qquad (5.10)$$

The values TR selected for our calculations were 100ms, 75ms, and 50ms. With the worst case (max and min) values of T_1 observed the error in quantifying N was determined.

5.8.2 Correction for variations in T_2

To calculate errors in signal intensity due to choice of TE and T_2 alone we chose TR as very large in equation 5.9 which gave us signal intensity depentent only on N, TE and T_2 and is given by the following equation.

$$S = N\left(S_f e^{-\frac{TE}{T_{2f}}} + S_s e^{-\frac{TE}{T_{2s}}}\right) \qquad (5.11)$$

87

We selected two possible ranges of TE *(i)* very small TE = 0.3ms, 0.6ms and 0.9ms *(ii)* long TE = 8ms. The errors in detecting sodium concentration i.e the loss in signal intensity during the echo delay, were determined for both cases using equation 5.11 and the variations in T_2.

Chapter 6

Results

Results reported here are for calf epiphyseal cartilage (EP) from distal ulna joint and calf articular cartilage (AC) from calf femoropatellar grove. Averaged results are represented as mean ± standard deviation.

T_1 and T_2 relaxation times for sodium in 150mM saline solution were found to be approximately equal with values ranging from 54 ms to 56 ms. The variations in the room temperature (25 ± 2 °C) were too small such that they are not expected to seriously affect the relaxation times. Repeated measurements of sodium concentration for calf EP cartilage plugs (n=6) varied by 3.9/6.6 percent [mean/max] with the samples frozen and re-equilibrated in between repeated measurements. The water content as determined by NMR varied by 3.4/7.3 (n=6) percent. Wet weights of same cartilage plug after freezing and requilibration varied by less than 2%. The repeatability of [Na^+] measurements on saline solution of 150mM NaCl were within 2% when measured on the same day.

6.1 Water Content

In order to relate sodium content as determined by area under NMR spectrum to sodium concentration inside cartilage tissue, water content of cartilage was determined by proton NMR spectroscopy. This water content as determined by proton spectroscopy correlates very well (r=0.98) with that determined by wet weight minus dry weight measurements assuming 1g = 1ml. The water content as determined by NMR was approximately 3 - 4 μl higher than that determined by wet weight minus dry weight measurements. (Figure 6.1). The dead time for the above results was set at 33.75 μsec.
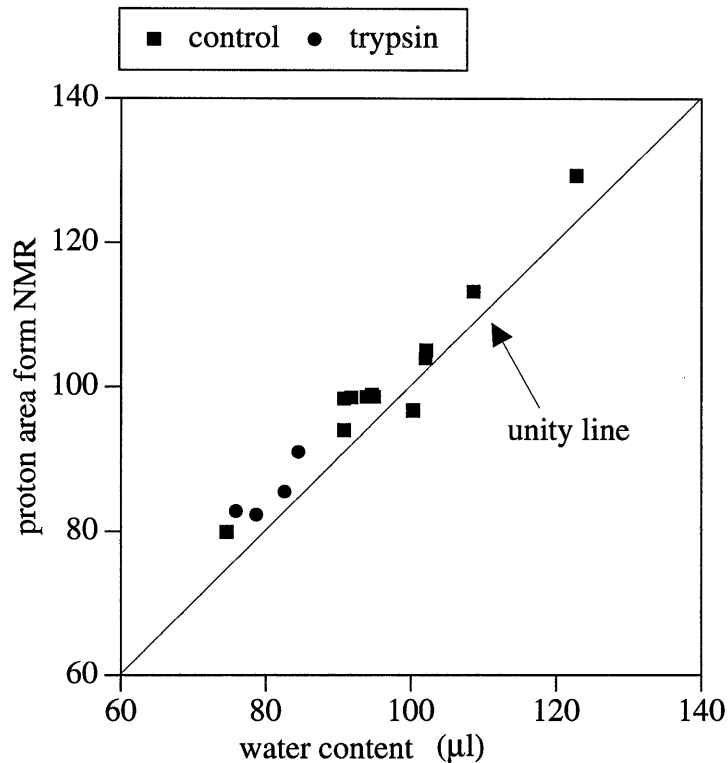
Figure 6.1: Cartilage water content as determined by area under proton NMR spectra as compared to water content as determined by wet weight minus dry weight measurements expressed in ml.

The receiver dead time was then varied to determine its effect on the quantitation of water content. The proton areas under the spectrum were then measured for both cartilge plugs and NMR standards with receiver dead times of 33.75, 65.0, 127.5, and 211.25 μsec to quantify water content. The results are shown in Figure 6.2 and summarized in Table 6.1. Increasing the dead time resulted in a decrease in estimate of water content in the cartilage as determined by NMR. This is due to the fact that area under the spectrum for cartilage and standard both decrease due to T_2 relaxation affects. T_2 in cartilage is much smaller than T_2 in solution. This would result in cartilage area to decrease more rapidly with increasing dead time thus resulting in a decrease in estimate of water content. While

a slightly greater estimate in water content at very short dead time of 33.75 μs may be due to the presence non-water protons.
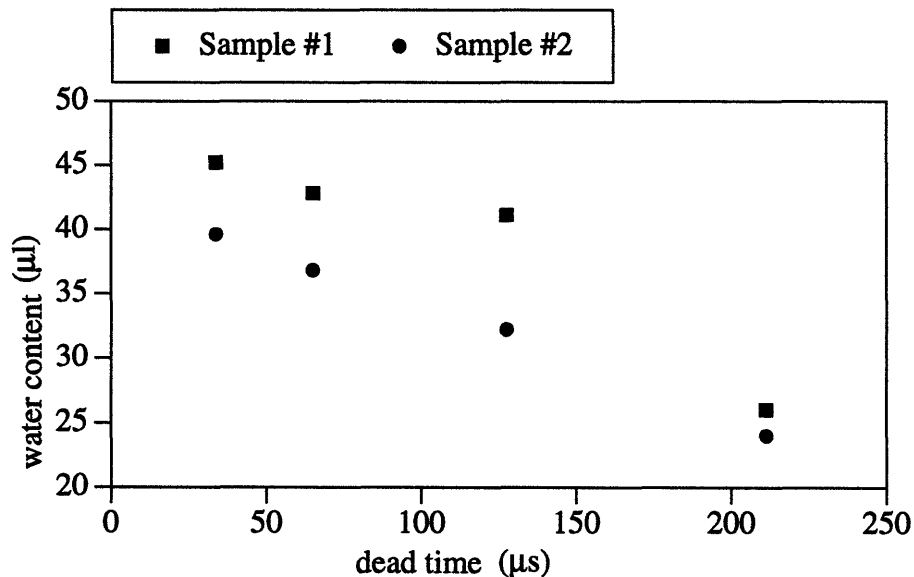
Figure 6.2: Cartilage water content as determined by NMR plotted versus dead time of the spectrometer. Long dead times result in decreased estimates of the water content.

	Sample # 1		Sample # 2	
Dead time (μs)	Water content (μl)	Water fraction (%)	Water content (μl)	Water fraction (%)
33.75	45.2	88.5	39.6	84.6
65.0	42.8	84.0	36.8	78.6
127.5	41.1	80.4	32.2	68.9
211.25	26.0	50.9	24.0	51.3
wet wt-dry wt	43.1	84.5	36.7	78.4

Table 6.1: The content of two EP cartilage samples as determined by NMR for varying dead times.The last row represents the water content as determined form wet weight minus dry weight measurements.

Tissue wet weights decreased significantly after trypsin digestion (Table 6.2). The ratio of tissue wet weights after trypsin digestion to that before was 0.77. This decrease in wet weight is due to decreased swelling pressure caused by proteoglycan removal and also by the actual decrease in the solid fraction of extracellular matrix. This decrease in solid fraction (removal of proteoglycans) results in a decrease in dry weight of the trypsin treated samples as compared to the control (Table 6.2).

Figure 6.3 shows total water content (ml) and water fraction (expressed as percentage of wet weight) measured for control and trypsinized cartilage. The values of control cartilage as determined by weights are normalized to one for both groups i.e. water content and water fraction values determined by weights are normalized to 1. The actual values of water content and water fraction are listed in Table 6.3.

Total tissue water content as determined area under proton spectrum and by wet weights minus dry weights decreased after trypsin treatment as compared to control (Figure 6.3), however the tissue water fraction (expressed as percentage of wet weight) increased by approximately 8%.

The water fraction for sequential slices is shown in Figure 6.4. For calf EP cartilage the slice number one is towards the metaphysis end while for calf AC cartilage the slices are numbered from the posterior end. All the slices examined were statistically similar in water content except for slice # 1 in case of epiphyseal cartilage from the distal ulna joint. This slice is closest to the metaphysis or growth plate.

For sodium concentration calculations in this study the water content as determined by wet weight minus dry weight was used. But our results indicate that water content as determined by NMR correlates with that determined by weight measurements. Thus NMR can be used as a nondestructive tool to determine the water content in cartilage.

	control	trypsin
wet weight (mg.)	127±8.2	97.3±8.5
dry weight (mg.)	25.3 3.3	12.7 0.9

Table 6.2: Cartilage wet weights and dry weights for control plugs and after trypsin treatment
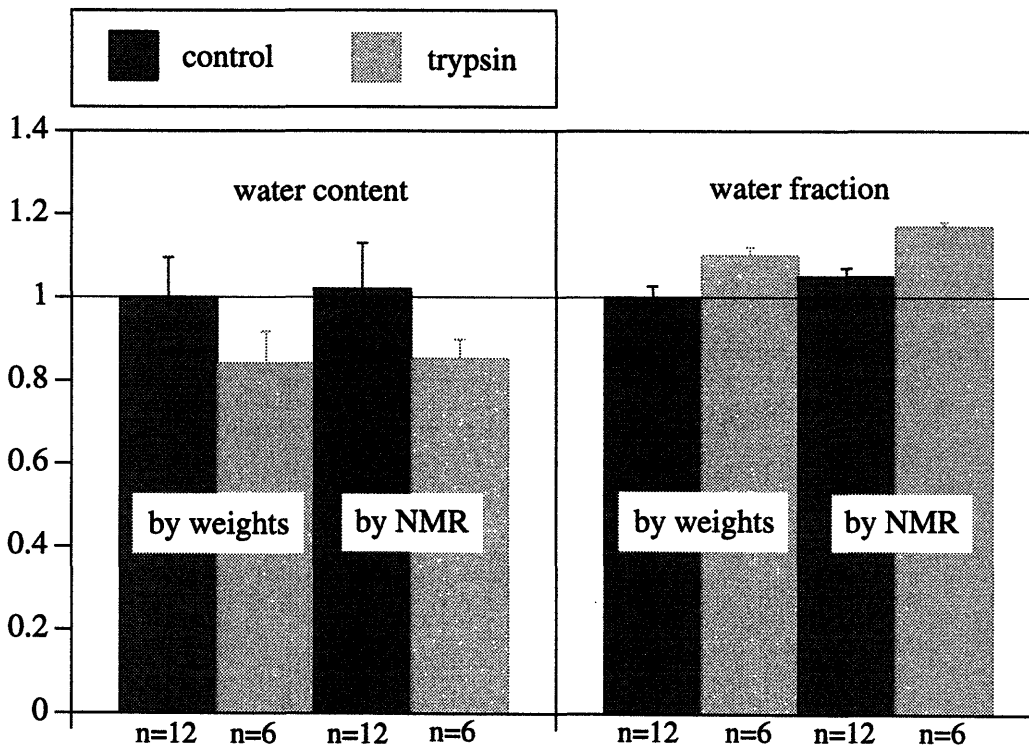
Figure 6.3: Total tissue water content (ml) and water fraction (expressed as percentage of wet weight) for epiphyseal cartilage before and after treatment with trypsin. The results shown here are for dead time of 33.75 μsec and it can be seen from the figure that the values determined by NMR are slightly higher than that determined by weights.

	control n=12		trypsin n=4	
calculated by	weights	NMR	weights	NMR
water content (μl)	100±9.5	102±11	84.5±7.7	85.5±4.7
water fraction (%)	78.9±2.2	82.8±1.6	86.9±1.5	92.6±1.0

Table 6.3: Comparison of absolute water content and tissue water fraction before and after trypsin digestion for epiphyseal cartilage.
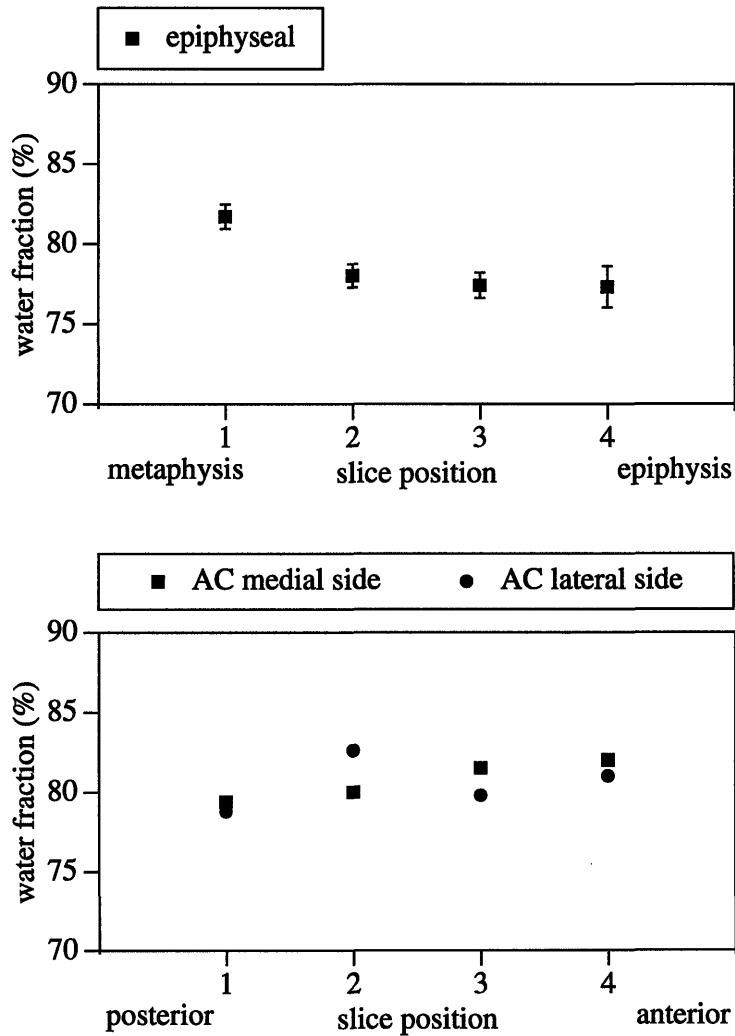
Figure 6.4: Tissue hydration (water content/wet weight) (a) calf epiphyseal cartilage, n=3. (b) calf articular cartilage, n=1.

6.2 Relaxation Time Results

6.2.1 T_1 results — Inversion recovery

The relaxation times for interstitial sodium were measured under control and pathologic interventions of trypsin and IL-1β treatment. The T_1 relaxation data when plotted on a semilogarithmic plot were linear and did not show any observable deviations from linear behavior after pathologic interventions (Figure 6.5); the data were fit to a single exponential. The possible range of T_1 for control EP cartilage was found to be 16 ms to 21 ms with a mean and standard deviation of 18.2 ± 1.7 ms (n = 14). The mean T_1 relaxation times increased to 32.2 ± 2.9 ms (n = 6) for trypsin treated EP cartilage. For one IL-1β treated EP cartilage plug the T_1 measured was 32.4 ms. The repeatability of T_1 measurements was within 6% (n=6).
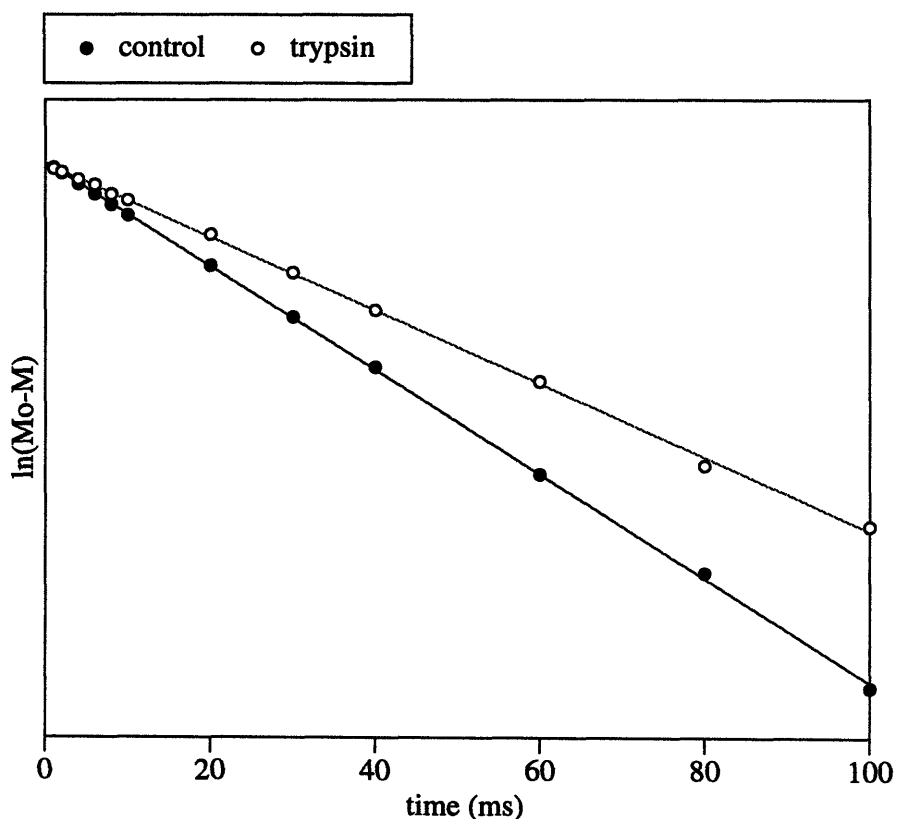
Figure 6.5: Typical T_1 from one EP cartilage plug under control and trypsin conditions. the first points are normalized to the same value.

6.2.2 T_2 results — Hahn echo

The measured T_2's for EP cartilage were clearly at least biexponential as seen by the nonlinear behavior on semi logarithmic plot (Figure 6.6). Examples of spectra used to obtain these types of curves are shown in Figure 6.7. The fast and slow T_2 components were derived from fitting T_2 data to a biexponential analysis fitting program. The corresponding component signal intensities are given as $M_f\%$ and $M_s\%$. The results of the fitting program are shown in Table 6.4. The repeatability (for six samples repeated twice) of measurement of T_2 relaxation parameters for control EP cartilage were within $T_{2f} = 5\%$; $T_{2s} = 12\%$; $M_f = 2\%$ and $M_s = 4\%$.

The biexponential behavior of sodium T_2 relaxation was also apparent for all samples treated with trypsin and IL-1β. T_{2f} component showed the most pronounced effect of degradation while fractional changes in T_{2s} were small. T_{2f} relaxation time decreased to 0.20 ± 0.06 ms (n = 6; 5 matched samples) for trypsinized cartilage and to 0.57 ± 0.07 ms (n = 3; no matched samples) for IL-1β treated cartilage. This fast T_2 decay in case of trypsinized cartilage is associated with the broad component of the spectrum (Figure 6.7b) and is seen to disappear in less than 1 ms echo delay.

Intratissue sodium ion concentration as measured by NMR showed a gradient as a function of position of explant for calf EP Cartilage (Figure 6.8). The range of values of sodium concentration observed was 0.3M (for slices near metaphysis) to approximately 0.45M (for slices near epiphysis). The values given are not corrected for invisibility which is 5% for the control plugs under these conditions (see results below). The fixed charge density shown in Figure 6.8 is calculated using ideal Donnan theory and the measured values of $[Na^+]$. T_2 fast did not show any distinct variations with the changes in sodium concentration for calf EP cartilage (Figure 6.8). The results are summarized in Table 6.5.

Calf articular cartilage specimens were similar in sodium hence proteoglycan concentration for sequential slices taken from posterior towards anterior end. The plugs were also similar in [Na$^+$] when taken from the medial or lateral side (Figure 6.9). The sodium concentration found for all plugs combined (i.e. medial and lateral) was 324 ± 13 (n=8) [mean $\pm$ sd]. T_{2f} in case of articular cartilage showed a strong dependence on the position of explant (Table 6.6 and Figure 6.9). The samples were similar in the slow T_2 component, 25.8 ± 1.4 [mean $\pm$ sd]. The magnitudes of the fast relaxation component ($M_f = 72 \pm 1.4$), and the slow relaxation component ($M_s = 28 \pm 1.4$), were also similar.

	control	trypsin	control	IL-1β
n	12	6	2	3
M_f (%)	70.0 ± 2.1	59.6 ± 2.8	65.5 ± 1.6	62.9 ± 2.0
M_s (%)	30.0 ± 2.1	40.4 ± 2.8	34.5 ± 1.6	37.1 ± 2.0
T_{2f} (ms)	0.96 ± 0.15	0.20 ± 0.06	1.3 ± 0.2	0.57 ± 0.07
T_{2s} (ms)	21.1 ± 2.9	23.9 ± 2.2	25.5 ± 0.8	25.6 ± 1.1

Table 6.4: EP cartilage sodium relaxation parameters. The controls in second set were kept in DMEM culture medium for ten days, and IL-1β treated cartilage were also kept in DMEM culture medium supplemented with IL-1β before the T_2 experiments were done. There are 5 matched samples in case of trypsin treated group and no matched samples in case of Il-1β treated group.
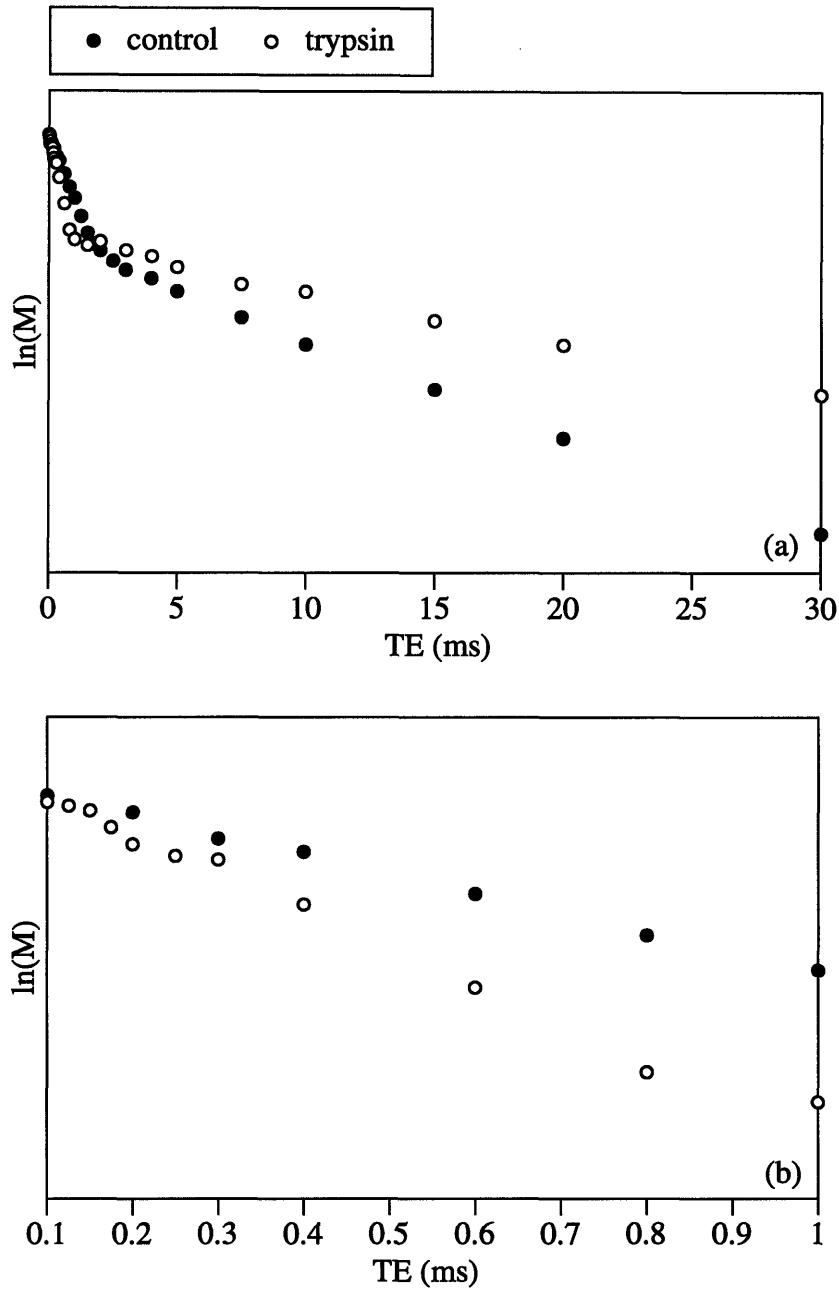
Figure 6.6: (a) T_2 relaxation curves for interstitial sodium in cartilage. (b) The fast T_2 component for cartilage under control and trypsin treatment. Open symbols in case of trypsin treated cartilage are seen to decay in magnitude more rapidly for shorter times than control indicating short T_2 fast relaxation time for trypsinized cartilage as compared to control.

0.05 0.1 0.2 0.3 0.4 0.6 0.8 1.0 1.25 1.5

1.75 2.0 2.5 3.0 4.0 5.0 7.5 10 15 20 30

(a)

0.01 0.02 0.04 0.06 0.08 0.1

0.125 0.15 0.175 0.2 0.25 0.3 0.4

0.6 0.8 1.0 1.5 2.0 3.0 4.0 5.0 7.5 10 15 20 30

(b)
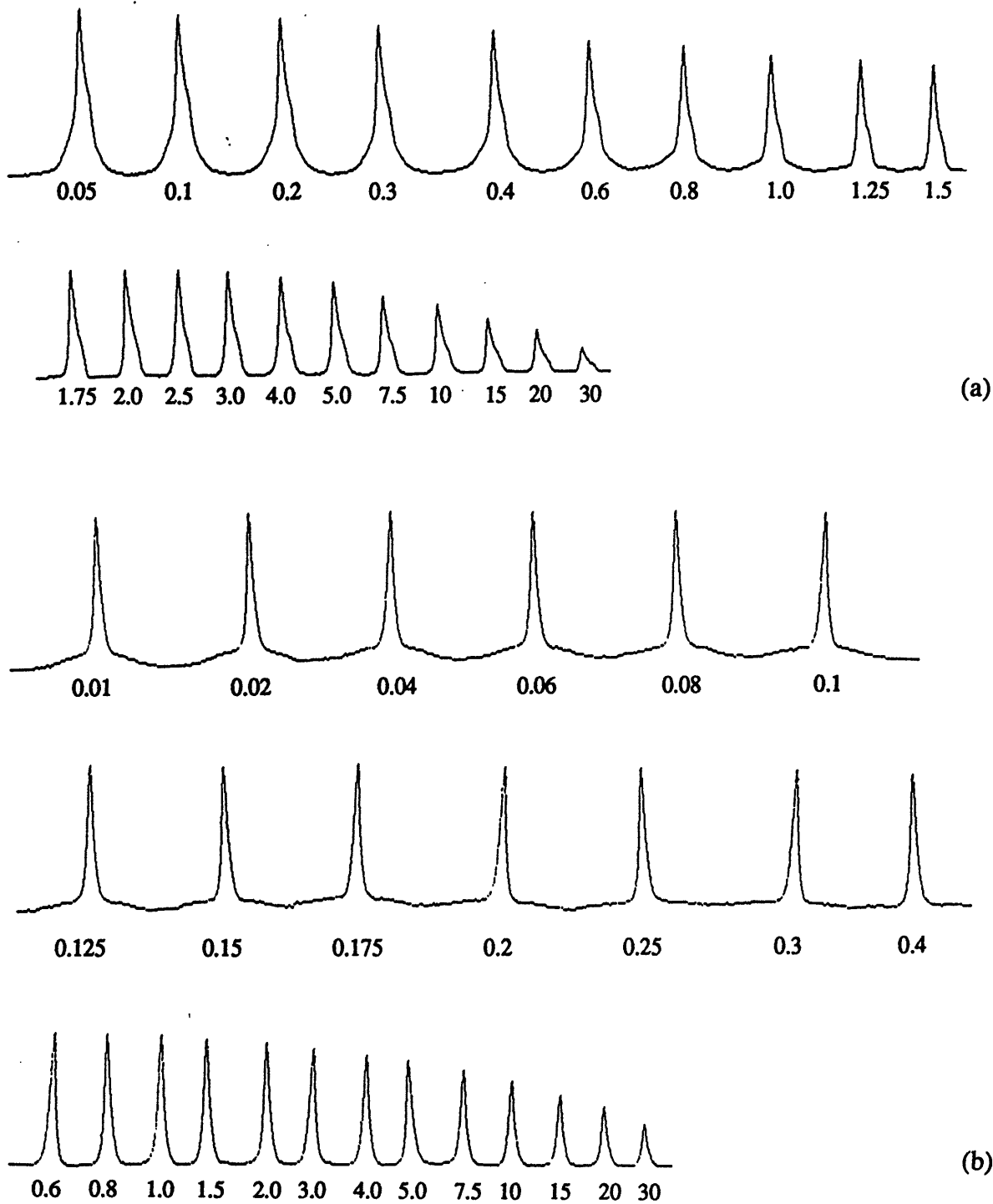
Figure 6.7: The resonance spectra obtained for T_2 measurement. The numbers correspond to echo times (a) Control; number of scans = 1000; (b) trypsinized cartilage; number of scans =2000. The broad component visible for short echo times correspond to fast T_2 decay and is seen to vanish in less than 1 ms. Data was collected at spectral width of 10000 Hz.

slice #	[Na] (mM)	FCD (mM)	T_{2f} (ms)
1	311.7 ± 11.9	-239.4 ± 14.7	0.87 ± 0.08
2	357.7 ± 3.4	-294.8 ± 4.0	1.05 ± 0.12
3	395.0 ± 7.4	-338.0 ± 8.4	0.99 ± 0.12
4	435 ± 10.2	-383.3 ± 11.4	1.13 ± 0.06

Table 6.5: Sodium concentration, FCD, and T_{2f} for sequential EP cartilage slices (numbered from metaphysis to epiphysis) taken from calf ulna joint (n=4).

slice #	medial		lateral	
	Na (mM)	T_{2f} (ms)	Na (mM)	T_{2f} (mM)
1	322.8	0.37	351.4	0.53
2	312.7	0.58	321.5	0.83
3	320	1.00	344.7	1.89
4	304.5	1.62	304.5	1.04

Table 6.6: Sodium concentration and T_{2f} relaxation component for AC. The medial and lateral plugs were taken from different joints. Slices are numbered from the posterior to anterior.
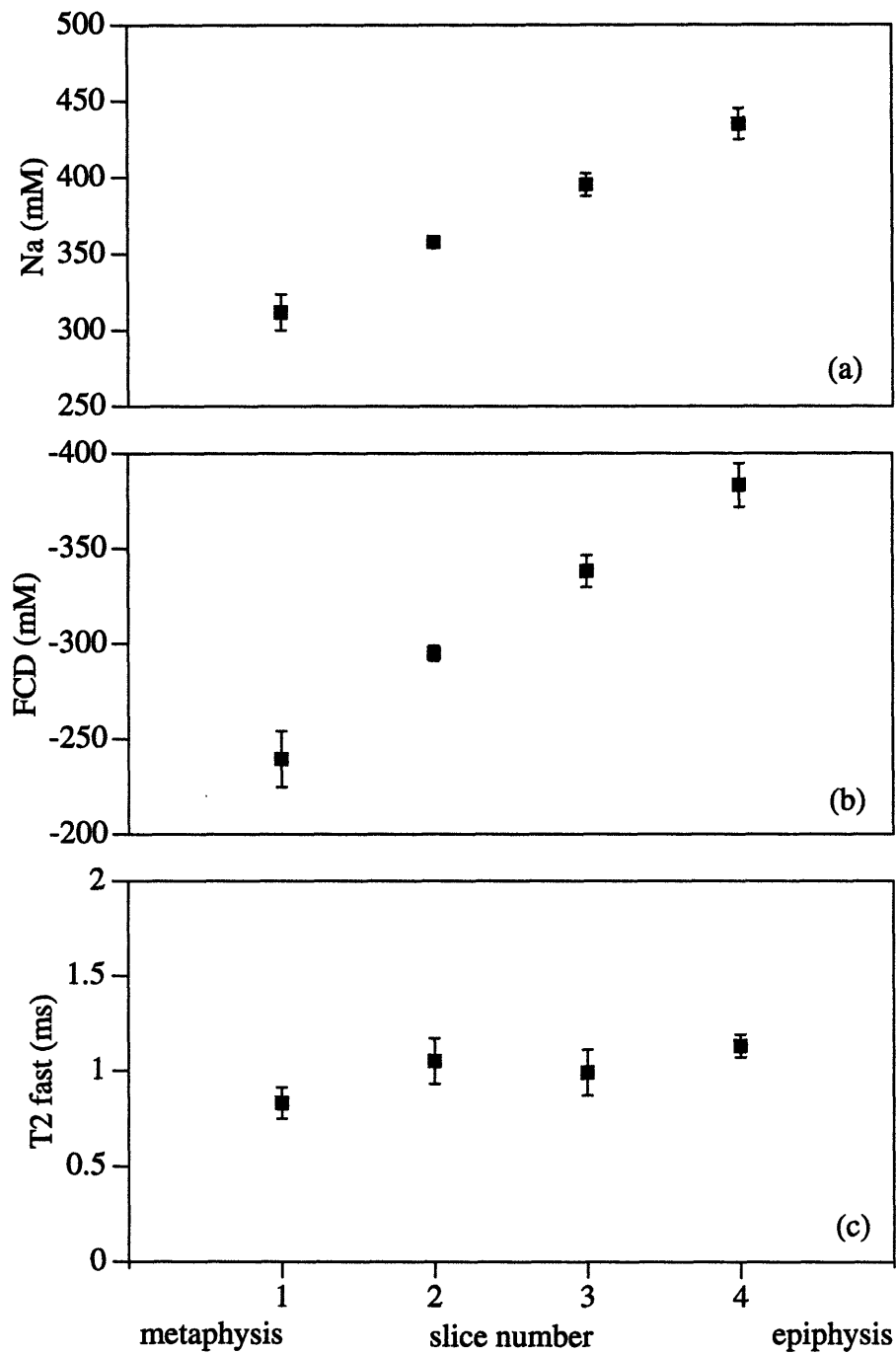
Figure 6.8: Sequential slices from distal ulna joint. (a) Sodium concentration. (b) FCD calculated by ideal Donnan theory. (c) Fast spin-spin relaxation component. The corresponding water fraction is given in figure 6.4.
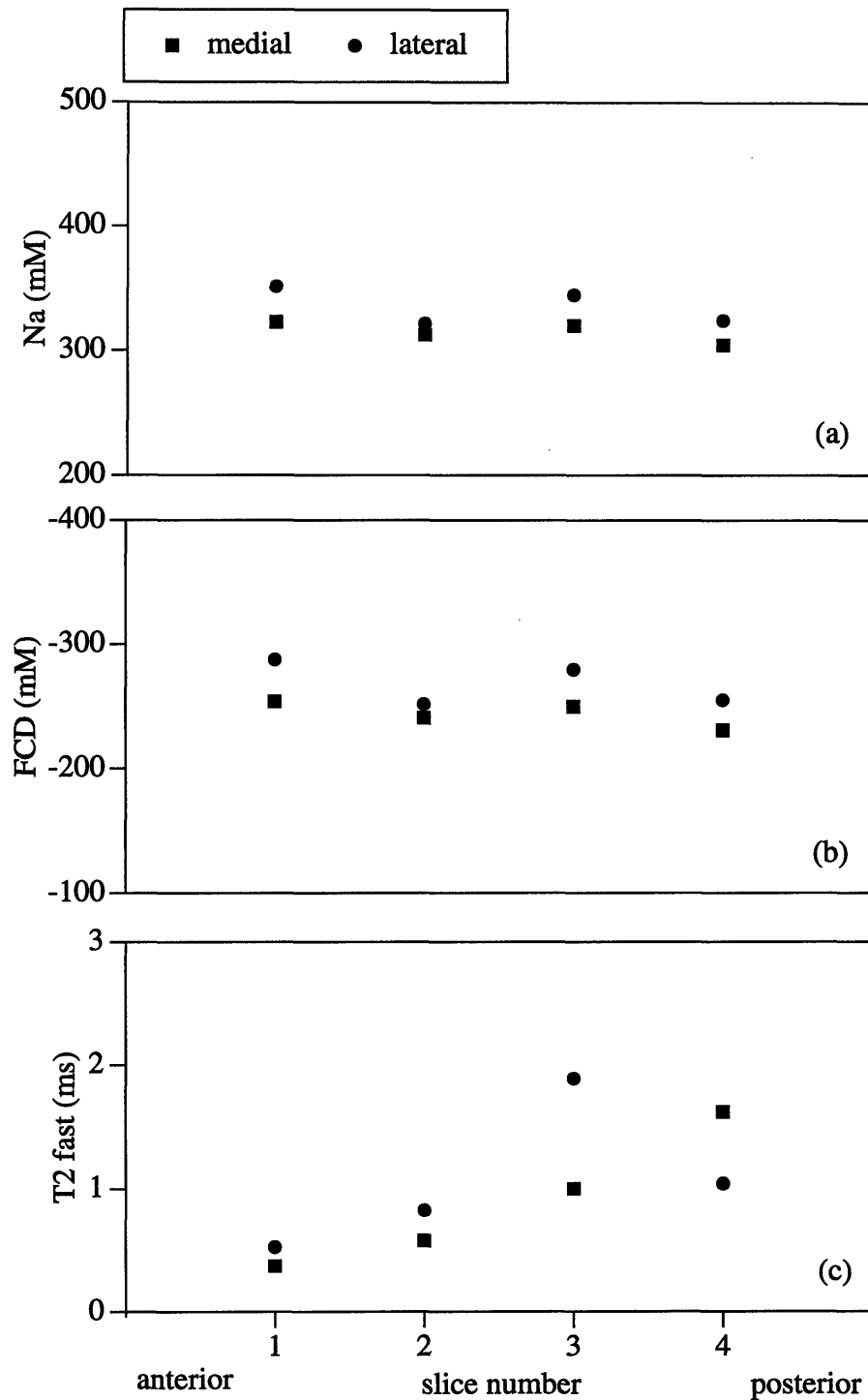
Figure 6.9: Sequential slices from femoropatellar grove. The medial and lateral slices were taken from different joints. (a) Sodium concentration. (b) FCD calculated by ideal Donnan theory. (c) Fast spin-spin relaxation component.The corresponding water fraction is given in figure 6.4.

6.2.3 T_{2fast} results measured by varying dead time

T_{2f} determined by varying the dead time for control EP cartilage (n=2) was found to be 1.11 ± 0.03 ms. This value agrees with 0.96 ± 0.15 ms determined by Hahn-echo pulse sequence for control samples (The two sets of controls i.e for dead time experiments and Hahn-echo experiments are not matched). The fast component for trypsin treated EP cartilage plugs as measured by varying the dead time is given in Table 6.7. The parameters were obtained by curvefitting the data to equation 5.6. The error caused by not including the slow decay is less than 0.1% at the short dead times used for this study. A bigger source of error is in recording the areas as there is pulse break through in the FID making it extremely difficult to set the base line.

### 6.2.4 T_{2f} vs. Linewidth Measurements

The line broadening due to the inhomogeneities in the magnetic field did not allow the fast and slow components to be clearly differentiated for control cartilage plugs therefore the linewidths for control plugs were not determined. For trypsinized cartilage the usual line widths for broad components (Figure 5.4) were on the order of 1500 Hz, and the two components were easily differentiated. The typical spectra are shown in Figure 6.10 below.

The line widths for these broad components were determined at half height. The contribution of the inhomogeneity broadening is small (less than 10%) compared to usual line widths observed and its effect is neglected. The results are listed in Table 6.7 along with the values measured by spin-echo techniques. The results correlate with each other very well. It is noted that for samples which had relatively longer decay times, T_{2f} component as determined by line widths is slightly smaller than that measured by Hahn echo. Since by line widths we are actually recording T_2^* therefore there is some additional broadening of the interstitial sodium which can be compensated by using spin echo.

sample	Hahn echo	dead time	Line width
1	0.23		0.18
2	0.16	0.17	0.17
3	0.5	0.40	0.40
4	0.31	0.33	0.27

Table 6.7: T_{2f} values for trypsinized cartilage as determined for EP cartilage by different methods. All values given are in ms.

SW = 10000 Hz
DE = 0.065 ms

SW = 20000 Hz
DE = 0.0335 ms

SW = 30000 Hz
DE = 0.02375 ms

SW = 50000Hz
DE = 0.015 ms
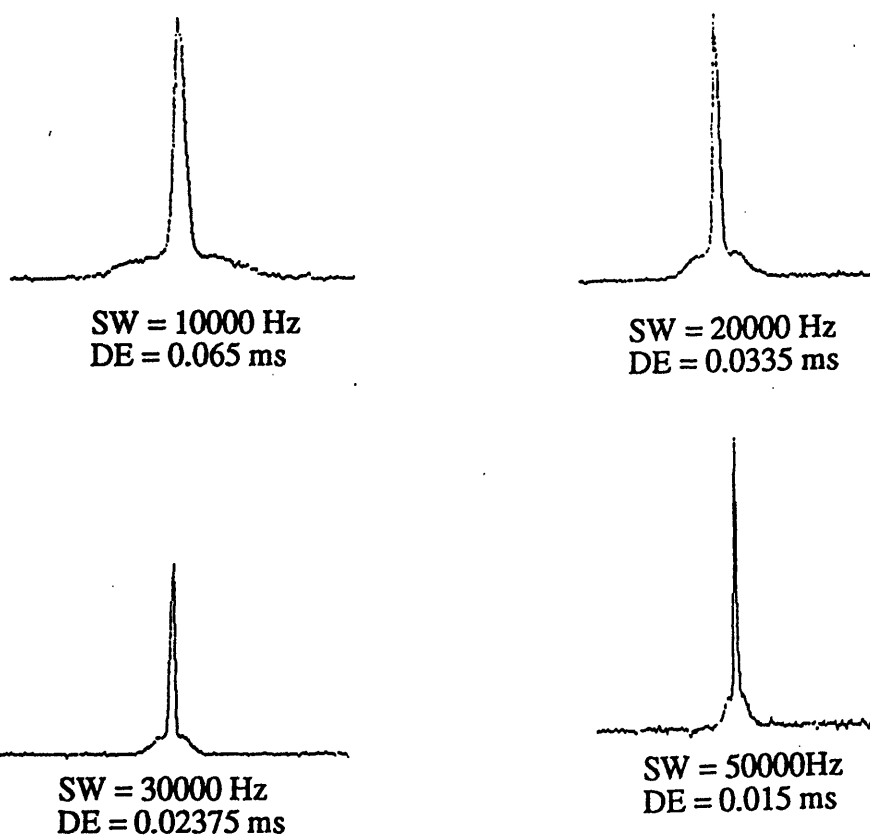
Figure 6.10: One pulse spectrum for linewidth measurements. The window width was the same for all spectra. The window height is adjusted to accommodate the spectrum. Line broadening of 20 Hz was used in processing these spectrum.

6.3 Desorption Studies

When KCl was used to desorb sodium, the area under the spectrum of cartilage plus KCl increased as compared to that of cartilage alone. This increase in area after desorption was used to calculate the invisibility fraction of sodium ions in cartilage.

The invisibility fraction determined for 2 control EP cartilage plugs at a dead time of 65 μs was found to be 5.7 $\pm$ 0.5% and the percentage invisibility observed for the trypsinized EP cartilage samples was (n = 3) was 14.9 $\pm$ 1.5% using desorption studies. 5% of sodium was found to be invisible for control cartilage and 17% for trypsinized cartilage plugs using the calculations based on T_2 measurements (Section 5.6).

Close to 5% of sodium was observed in the cartilage plugs after removal from KCl. Approximately 10% of sodium was expected in the trypsinized cartilage plugs and greater than 10% was expected in control plugs based on the volume of desorbing solution used. Since most of the sodium is removed from the cartilage after desorption (~90%) the signal to noise ratio for the left over sodium signal is extremely low making it difficult to accurately determine the area under the spectrum. Also the left over sodium in the cartilage may still be partially invisible due to relaxation affects thus resulting in this difference.

6.4 T_2 Dependence on Orientation

For 3 cubic EP cartilage plugs held in the NMR tube with the longitudinal axis parallel and perpendicular to the magnetic field the spin-spin relaxation times are shown in Table 6.8. T_2 fast values were approximately 50% greater when the cartilage piece was held with its axis parallel to the magnetic field as compared to perpendicular orientation.

For the spherical EP cartilage plug the spin-spin relaxation time was determined for orientation angles at increments of 10°. The 0° angle corresponds to the case when the longitudinal axis (Figure 5.3) is parallel to the magnetic field. The magnitudes of the fast and slow components did not show any strong variations with the orientation angle and were $63.1 \pm 1.8\%$ and $36.9 \pm 1.8\%$ (mean $\pm$ sd) respectively. The range of values for slow relaxation component was 18 ms to 21 ms with a mean/sd of 19.4 ± 1.3 ms.

The fast T_2 component showed strong variations with the orientation angle with values ranging from 1 ms to 1.7 ms (Figure 6.11). The difference in T_{2f} for the orientations of 0° and 30° clearly is evident when the typical T_2 relaxation data is plotted on a semi-logarithmic plot (Figure 6.12). The first point was normalized to the same value. The data points weighted by the slow component (for times greater than 5ms) fall approximately on each other for both orientations (Figure 6.12a) indicating that the slow component is not strongly affected by orientation.The data points weighted by the fast component (for times less than 2.5 ms) decreases rapidly for 0° orientations (Figure 6.12b) indicating shorter T_2 fast for this orientation. Because of difficulty in handling the trypsinized cartilage, and low signal to noise ratio the orientation dependence for trypsinized cartilage plugs was not studied.

	axis perpendicular	axis parallel
n	3	3
M_f (%)	69.7 ± 1.04	63.6 ± 0.9
M_s (%)	30.3 ± 1.04	36.4 ± 0.9
T_{2f} (ms)	0.91 ± 0.26	1.40 ± 0.15
T_{2s} (ms)	22.1 ± 1.3	17.8 ± 0.21

Table 6.8: Spin-spin relaxation time for two orientations. 4 mm cubic EP cartilage plugs were used.
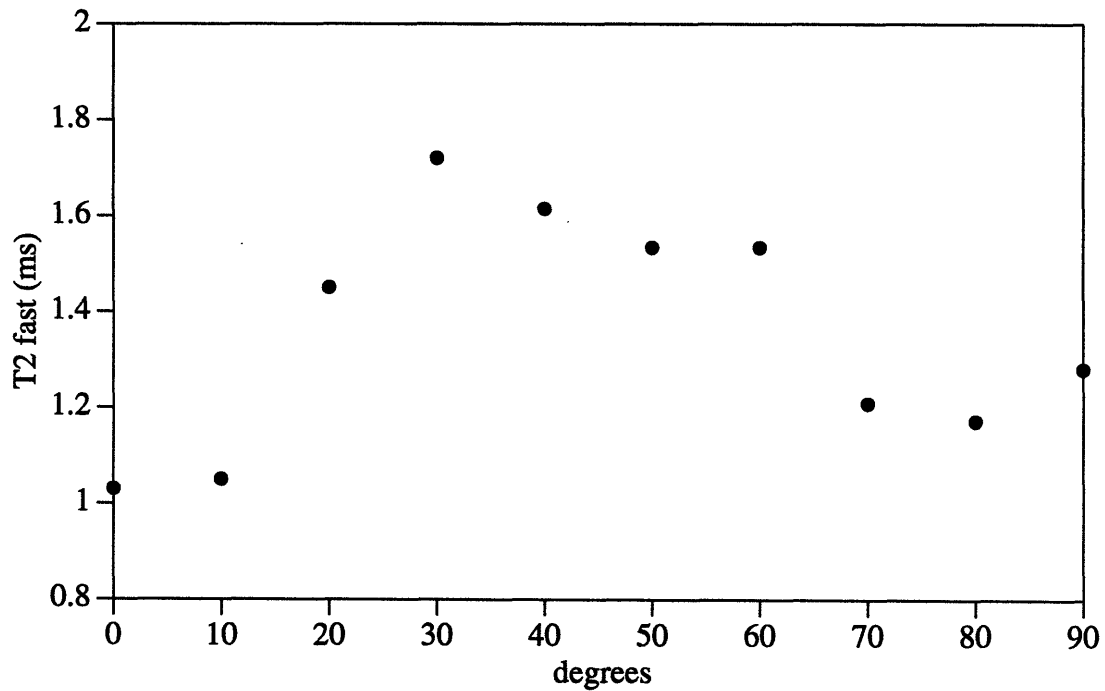
Figure 6.11: Orientation dependent relaxation behavior relative to static magnetic field. The results are for T_2 fast component a EP spherical sample.
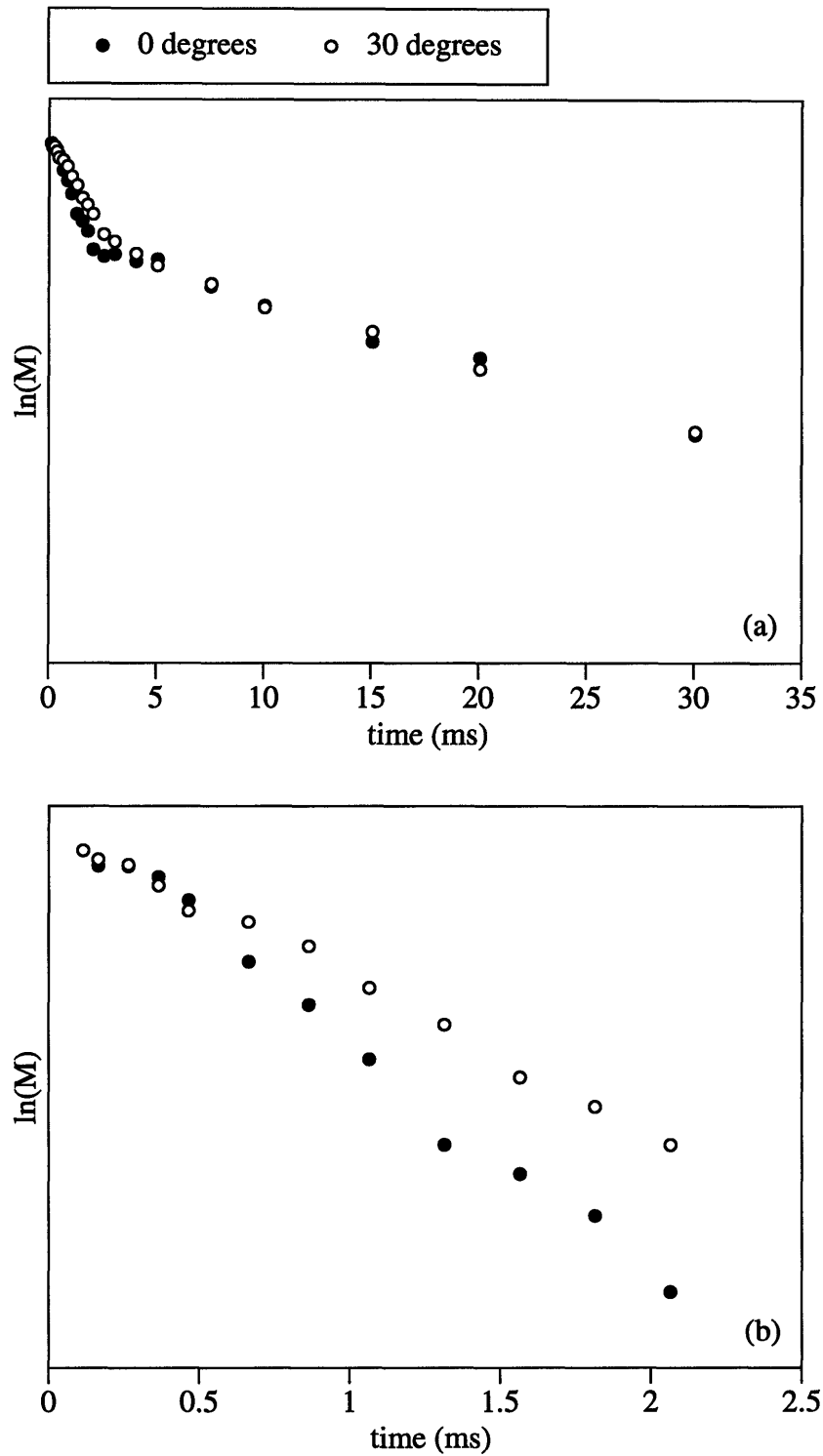
Figure 6.12: T_2 data for spherical sample. (a) Complete T_2 data points. The points for longer times fall on each other indicating same T_{2s}. (b) Data points for the shorter times. The points at $0°$ orientations decrease in magnitude more rapidly indicating short T_{2f}.

6.5 Implications for MR Imaging

6.5.1 Correction for variations in T_1

The worst case values of T_1 observed were 16 ms (for control cartilage) and 35 ms (for degraded cartilage). If we choose TR as 100 ms, 75 ms, and 50 ms as reported earlier the effect of variations in T_1 on signal intensity is shown in Figure 6.13. A reference signal intensity of 100 is chosen for the case when there is no saturation of signal i.e when $T_1 = 0$ or TR is very large as compared to T_1. It can be seen from Figure 6.13 that selecting smaller TR results in a greater variations in signal intensity and the loss of signal intensity due to saturation effects is more.
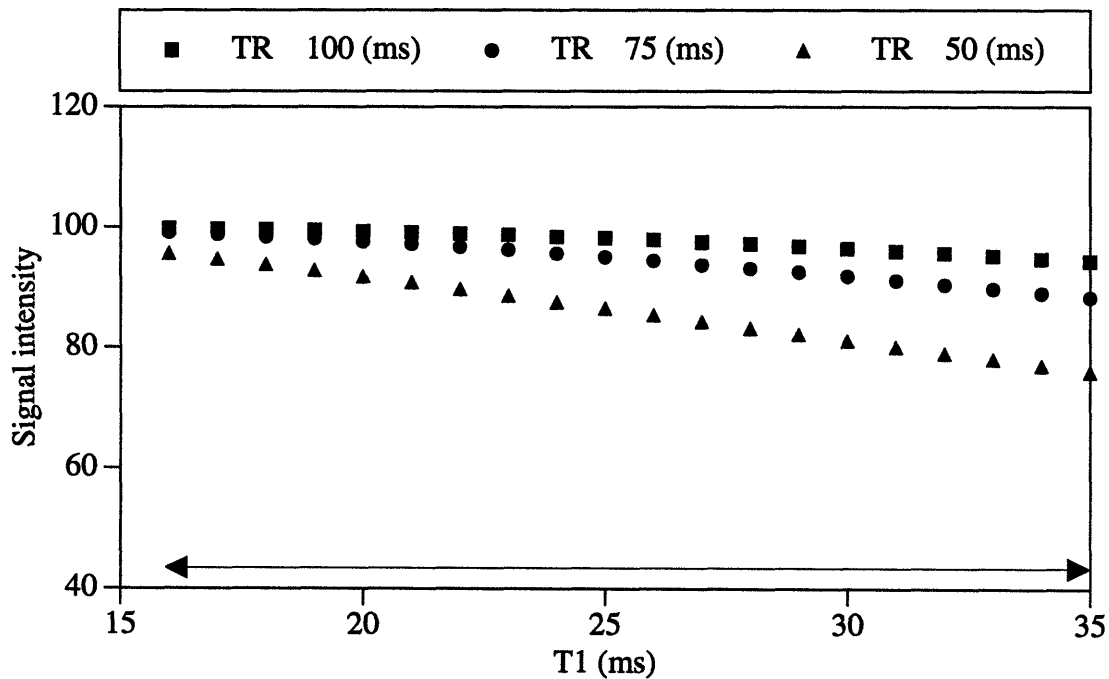
Figure 6.13: Signal intensity variations for the observed changes in T_1. For shorter TR's more signal is lost due to saturation effects and the variations in signal intensity are more for the given range of T_1 values.

As can be seen from the Figure 6.13, that at repetition time of 100 ms and with T_1 in range of 16 ms to 35 ms the signal intensity goes from 99.8 to 94.3. Thus if we choose an average T_1 of 28 ms the signal intensity would be 97.2 and the percent error on the calculation of sodium concentration will be on the order of 3% due to the variations in T_1. A choice of TR = 50 ms and average T_1 of 26 ms would result in signal intensity of 85% and a maximum error of 11% in calculating sodium ion concentration. The results are summarized in Table 6.9.

TR (ms)	max error (%)	saturation loss (%)
50	11	15
75	6	6
100	3	3

Table 6.9: Maximum errors observed for worst case variations in T_1 and the saturation loss due to fast repetition time for experimentally feasible TR's selected.

6.5.2 Corrections for variations in T_2

There are two available options of choosing a short TE and long TE as mentioned in section 5.8.

(i) Short TE's:

For a given TE, variations in T_{2f} and T_{2s} limit our ability to quantify sodium ion concentration. Since ~65% of the signal decays with fast time constant therefore changes in fast time constant is more likely to affect our results for short TE's. Figure 6.14 shows variations in signal intensity for the observed variations in T_{2f} and chosen TE's of 0.3 ms,

0.6 ms, and 0.9ms. The reference image intensity of 100 is chosen when no signal is lost during the echo delay i.e either TE = 0 ms or T_2 is much greater than TE.
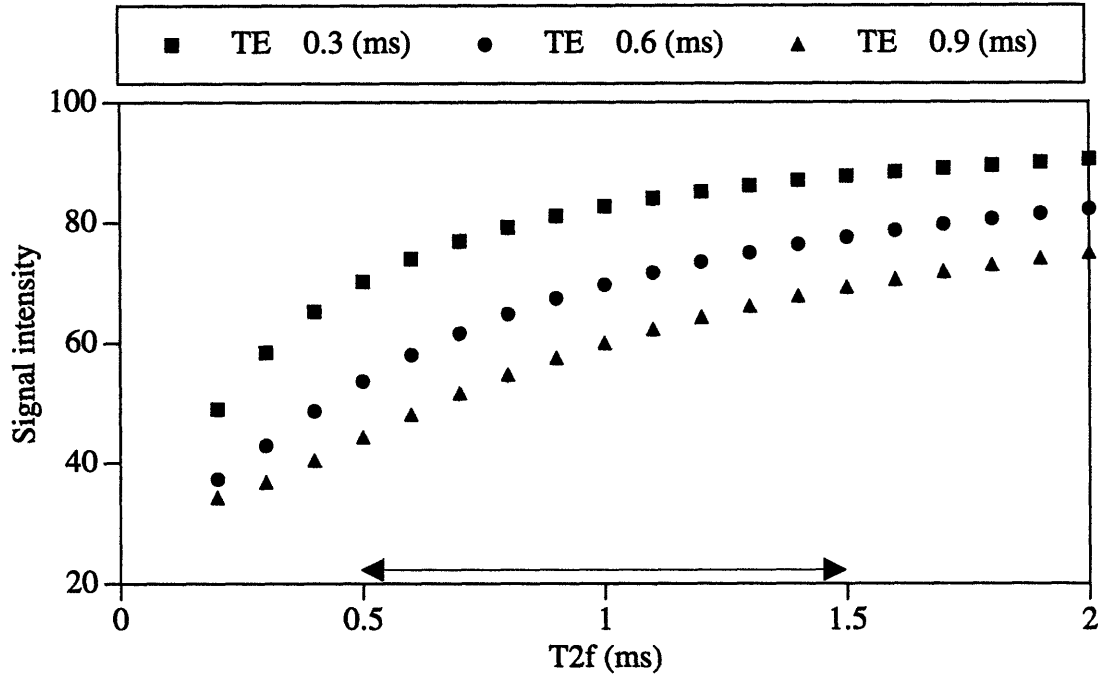
Figure 6.14: Signal intensity variations for the observed changes in T_{2f}. T_{2s} is taken to be 21 ms and the relative intensities of T_{2f} and T_{2s} as 0.65 and 0.35 respectively. The arrow represents the expected variations in T_{2f}.

T_{2f} was generally seen to vary from 0.5 ms to 1.5ms. The error due to this variation on calculation of sodium concentration was calculated as follows. For a choice of TE = 0.3 ms the signal intensity varies from 70.2 to 87.7 for the above range of values of T_{2f}. A choice of average T_{2f} = 0.8 ms would result in a signal intensity of 79.2 and would result in percent error on the order of 11% in calculating sodium concentration. A longer TE = 0.9 ms and average T_{2f} = 0.9 ms would result signal intensity of only 58% and corresponding error on the order of 23%. The results are summarized in Table 6.10.

TE (ms)	max error (%)	signal loss (%)
0.3	11	20
0.6	20	35
0.9	23	44

Table 6.10: Maximum errors that would be observed and the loss in signal intensity for given TE's.

(ii) Long TE's:

If TE = 8 ms is chosen then the contribution of the fast component to signal intensity has decayed to zero and any variations in the fast relaxation component would not affect our calculations. At this echo time of 8 ms the changes in T_{2s} (16 ms to 28 ms) observed would result in an worst case error of 12% for a choice of average T_{2s} of 20 ms. At this choice of TE only 24% of the signal is available and this would drastically reduce the signal to noise ratio.

Chapter 7

Discussion

7.1 Discussion of Results

In this study we have characterized the NMR relaxation parameters of sodium in the interstitial fluid of cartilage. The effect of the measured relaxation times on our ability to quantify sodium ion concentration in MR imaging was also studied.

To summarize the results, sodium T_1 was measured by the inversion recovery pulse sequence and consisted of a single exponential. T_1 values were measured to be approximately 20 ms for control EP cartilage and increased to over 30 ms for pathologically degraded cartilage. Similar changes in T_1 were also observed by L.A. Jelicks et al [1993] for bovine nasal cartilage.

The measurement of T_2 indicated the presence of both a fast and a slow component. The best biexponential fit gave time constants of approximately 1 ms and 20 ms with relative fractions of 0.65 and 0.35 respectively. The fast component of T_2 was strongly affected by the pathologic degradation of cartilage to values of approximately 0.2 ms with trypsin treatment and 0.5 ms with interleukin-1β treatment. The fractional changes in the slow component were not significant. The T_2 data were fit with a sum of two exponentials because a single exponential did not adequately fit the data. A fit of the data to a sum of more than two exponentials was not justifiable by the number of data points observed. The number of data points was restricted by the low signal to noise ratio for sodium.

We found T_1 to vary between 16 ms and 35 ms for control and degraded cartilage. Our results indicate that if we choose an imaging of parameter TR = 100 ms, and an average T_1 of 28 ms we would be able to calculate the sodium ion concentration inside the tissue to within 3%. A correction factor of 0.97 is required for above choice of imaging conditions

because saturation effects would result in a loss in signal intensity of 3%. A shorter choice of TR is not desirable because it would cause a greater percentage error in calculating sodium concentration.

The choice of an imaging parameter TE = 0.3 ms is desirable to quantify sodium concentration inside the tissue. Uncertainties in T_{2s} will not affect the calculated signal at such a short echo delay. Variations in T_{2f} from 0.5 ms to 1.5 ms would cause a percentage error on the order of 11% in calculation of sodium concentration given assumed average T_{2f} of 0.8 ms. A correction factor of 0.8 is required to correct for the signal decay during the echo delay.

The invisible fraction of sodium as measured by our desorption studies agreed with that calculated from T_2 data. This confirms that the measured T_2 represents all of the mobile sodium in the tissue. Thus the above given correction factor of 0.8 is an appropriate choice to compensate for signal decay during TE, which we have calculated using T_2 measurements.

The errors mentioned above, due to the variations in T_1 and T_2, are relatively small compared to the changes which we would expect during pathologic changes in the tissue.

7.2 General Comments

The most significant changes were observed in the T_{2f} component of transverse relaxation. T_{2f} values decreased significantly with the removal of proteoglycans from the cartilage matrix. The removal of proteoglycans causes a decrease in fixed charge density of the tissue. This results in a decreased tissue sodium ion concentration as required by Donnan equilibrium [Maroudas A. 1979]. In case of complete removal of proteoglycans the sodium ion concentration changes by 50% - 70% from control values.

114

Tissue proteoglycan content and hence sodium ion concentration in case of epiphyseal cartilage also has natural variations. [Na^+] was seen to increase by 35% form metaphysis to epiphysis end. T_{2f} did not show any consistent variations with this natural changes in sodium concentration. In contrast articular cartilage plugs which were similar in [Na^+] did show strong variations in the fast component with the position of plug ranging in values form 0.4 ms to 1.7 ms.

Jelicks et al [1993] measured T_1 and T_2 (of the narrow line corresponding to the slow component in our study) for sodium in bovine nasal cartilage. They observed that both T_1 and T_2 components increased with degradation of cartilage. They concluded that as water fraction increases with cartilage degradation the sodium ions become more mobile resulting in an increase in relaxation times. Our results of T_{2f} indicate that the increase in mobility of sodium ions is not the only factor responsible for the increase in relaxation times since in this case our T_{2f} component would also increase. Also the changes in the relaxation times should not be directly linked to changes in the sodium ion concentrations after degrading the cartilage. The relaxation times are dependent on the changes in the magnitudes and rates in the fluctuations of the local electric fields. Treating cartilage with trypsin and IL-1β results in changes collagen structure and water content along with the removal of proteoglycans. This may cause changes in the correlation times, and in the population fractions and exchange rates of different compartments causing changes in the relaxation times.

Another observation was a strong dependence of T_{2f} on the orientation of the cartilage sample with respect to the magnetic field. This dependence of T_2 on the orientation can be due to either or both of the following possibilities first cartilage consists of a network of oriented collagen fibers as seen on electron microscope [Bloom and Fawcett 1962]. These

oriented collagen fibers can cause local changes in magnetic susceptibility which can result in different T_2 relaxation times.

Second, Shimizu H. [1964] showed that spectral densities has a complicated dependence upon molecular motions and that the spectral densities, and hence relaxation times, are dependent on orientation angle. Woessner D.E. [1991] also mentioned that the mathematical terms for electric quadrupole relaxation have the same orientation dependencies as the magnetic dipolar relaxation. Eliav and Navon [1993] suggested that in cartilage slow anisotropic diffusion around collagen fibers and perpendicular to them may cause the spectral densities to be dependent on the angle between the local directors and magnetic field indicating that the relaxation rates in the cartilage tissue depend on the orientation of the local director relative to the magnetic field.

7.3 Summary

Our studies indicate that T_1 and T_2 relaxation times of interstitial sodium in cartilage vary with pathologic states. Although these variations in relaxation times will affect our ability to quantify sodium concentration, with a suitable choice of imaging parameters this error in calculating sodium concentration can be made small compared to the expected changes in sodium concentration due to pathology.

Thus sodium MRI technique can be used to detect spatial variations in FCD for human samples in vivo. This will provide powerful means for observing progressive degeneration of cartilage tissue.

7.4 Future Considerations

Many opportunities exist for future studies. One would be to determine the physiological basis of sodium relaxation and quadrupolar interactions inside the tissue, i.e to deter-

mine which tissue matrix components affect sodium relaxation. This would require the use of model systems such as proteoglycan and collagen standards of different concentration and nature.

Compressing the cartilage results in a decrease in tissue water fraction and a decrease in tissue sodium content, but leaves the total number of charged groups inside the cartilage unchanged. This would mimics joint loading and would yield information about how joint loading of normal and degraded cartilage affects sodium relaxation times. Other perturbations include equilibrating cartilage in baths of different sodium ion concentrations and different pH.

In addition, the present study can be extended to in vivo imaging experiments. Previous applications of NMR to the study of cartilage have involved proton imaging aimed at producing images with improved contrast, higher signal to noise ratio, and finer resolution. These studies have diagnostic capabilities only when structural changes in cartilage occur, usually at an advanced disease stage. Our studies indicate that sodium MRI can be used as a quantitative diagnostic tool to diagnose the development and successive progression of degenerative cartilage diseases such as arthritis. This in vivo sodium MR imaging would require developing and exploring techniques for short echo time imaging.

Appendix A

Analysis of Relaxation Time Parameters

A.1 Methods

There are several possible models that can be used to describe the relaxation data as discussed in the theory section. In this analysis the model having one homogeneous pool of sodium, with the biexponential relaxation due to quadrupolar effects was analyzed. The parameters determined in the experiments were used in the equations 2.20 to 2.23 and rewritten below, to test the validity of the model.

$$\frac{1}{T_{1fast}} = 2\left(\frac{eQ}{\hbar}\right)^2 J(\omega_o) \tag{A.1}$$

$$\frac{1}{T_{1slow}} = 2\left(\frac{eQ}{\hbar}\right)^2 J(2\omega_o) \tag{A.2}$$

$$\frac{1}{T_{2fast}} = \left(\frac{eQ}{\hbar}\right)^2 [J(0) + J(\omega_o)] \tag{A.3}$$

$$\frac{1}{T_{2slow}} = \left(\frac{eQ}{\hbar}\right)^2 [J(\omega_o) + J(2\omega_o)] \tag{A.4}$$

where the relative magnitudes are 20% and 80% for fast and slow components of T_1 respectively and 60% and 40% for fast and slow components of T_2 respectively. $J(\omega)$ is given as

$$J(\omega) = \frac{(eq)^2}{20} \frac{\tau_c}{1 + (\omega\tau_c)^2} \tag{A.5}$$

where τ_c is the characteristic decay time of the correlation function. The two measured values of T_2 were used to determine the correlation time given the resonant frequency,

$\omega_o = 2\pi(95.26 \times 10^6)$ and then they were plugged into the equations for T_1 to determine the expected value of fast and slow T_1's as required by this model. Since the fast component of T_1 has only 20% of the total magnitude therefore it is difficult to resolve experimentally. Only a single exponential decay for T_1 was observed therefore the weighted average of T_1 as given by equation A.6 was calculated its agreement with the measured T_1 was then evaluated.

$$\frac{1}{T_1} = \frac{0.2}{T_{1fast}} + \frac{0.8}{T_{1slow}} \qquad\qquad (A.6)$$

A.2 Results

The values calculated as described above are summarized in the Table A.1 along with the measured values.

	control	trypsin	IL-1β
τ_c	8.46×10^{-9}	1.81×10^{-8}	1.23×10^{-8}
T_{1fast} (calculated)	13.3	15.0	16.0
T_{1slow} (calculated)	51.6	59.4	63.3
T_1 (calculated)	32.7	37.2	39.8
T_1 (measured)	18.2	32.2	32.4

Table A.1: Calculated and measured values for Na T_1 in cartilage

The results suggests that the data does not indicate to a single pool of ions for since calculated T_1 values are significantly different from the measured values.

Any models based on multiple sodium compartments and involving higher number of time constants cannot be uniquely fit with the number of data points observed. It should be noted that the parameters observed by biexponential fit are a characterization of sodium

decay in cartilage and not an absolute determination of time constants which may be

present.

References

[1] Adam G., Nolte-Ernsting C., Prescher A., Buhne M., Bruchmuller K., Kupper W., Gunther R.W., Experimental hayline cartilage lesions: two dimensional spin-echo versus three dimensional gradient echo MR imaging. JMRI 1991; 1:665-672.

[2] Antonopoulos C.A., Gardell S., Szirami J.A., De Tyssonsk E.R., Determination of Glycosaminoglycans (Mucopolysaccharides) from tissues on the microgram scale. Biochim Biophys Acta 1964; 83:1-19.

[3] Bitter T., Muir H.M., A modified Uronic acid Carbazole Reaction. Analytical Biochemistry 1962; 4:330-334.

[4] Bloom W, Fawcett D.W., A textbook of histology. W.B. Saunders Company Philidelphia, London 1962.

[5] Bongartz G., Bock E., Horbach T., Requardt H., Degenerative cartilage lesions of the hip. Magnetic resonance evaluation. Magn Reson Imag 1989; 7:179-186.

[6] Brendsen H.J.C., Edzes H.T., The observation and general interpretation of sodium magnetic resonance in biological materials. Annals New York Academy of Sciences 1973; 459-485.

[7] Buckwalter J., Hunziker E., Rosenberg L., Coutts R., Adams M., Eyre D., Articular cartilage: Composition and structure. American academy of orthopaedic surgeons, Park Ridge, IL, 1988; 405-425.

[8] Bull T.E., Nuclear magnetic relaxation of spin-3/2 nuclei involved in chemical exchange. J Magn Reson 1972; 8:344-353.

[9] Bull T.E., Andrasko J., Chiancone E., Forsen S., Pulsed nuclear magnetic resonance studies on ^{23}Na, ^{7}Li, ^{35}Cl binding to human oxy- and carbon monoxyhaemoglobin. J Mol Biol 1973; 73:251-259.

[10] Burk D.L., Kanal E., Brunberg J.A., Johnstone G.F., Swensen H.E., Wolf G.L., 1.5T surface coil MRI of the knee. AJR 1986; 147:293-300.

[11] Burstein D., Fossel E.T., Effect of temperature, buffer osmolarity and shift reagent concentration on the intracellular sodium and potassium relaxation times of red blood cells. J Magn Reson 1987a; 73:150-158.

[12] Burstein D., Fossel E.T., Intracellular sodium and lithium NMR relaxation times in perfused frog heart. Magn Reson in Med 1987b; 4:261-273.

[13] Burstein D., Mattingly M., Magnetic resonance imaging of intracellular sodium. J Magn Reson 1989; 83:197-204.

[14] Burstein D., Gray M.L., Hartman A.L., Gipe R., Foy B.D., Diffusion of small solutes in cartilage as measured by nuclaer magnetic resonance(NMR) spectroscopy and imaging. J Ortho Res 1993; 11(4):465-478.

[15] Chandnani V.P., Ho C., Chu P., Trudell D., Resnick D., Knee hyaline cartilage evaluated with MR imaging: A cadaveric study involving multiple imaging sequences and intraarticular injection of Gadolinium and saline solution. Radiology 1991; 178:557-561.

[16] Chang D.C., Woessner D.E., Spin-echo study of ^{23}Na relaxation in skeletal muscle. Evidence of sodium ion binding inside a biological cell. J Magn Reson 1978; 30:185-191.

[17] Cho Z.H., Jones J.P., Singh M., Foundations of medical imaging. John Wiley & sons, inc 1993.

[18] Crooks L.E., Hylton N.M., Ortendahl D.A., Posin J.P., Kaufman L., The value of relaxation times and density measurements in clinical MRI. Invest Radiol 1987; 22:158-169.

[19] Dayer J.M., Goldring S.R., Robinson D.R., Krane S.M., Effects of human mononuclear cell factor on cultured rheumatoid synovial cells. Interactions of prostaglandin E_2 and cyclic adenosine 3' , 5' - monophosphate. Biochem Biophys ACTA 1979; 586:87-105.

[20] DeLayre J.L., Ingwall J.S., Malloy C., Fossel E.T., Gated sodium-23 nuclaer magnetic resonance images of an isolated perfused working rat heart. Science 1985; 212:935-936.

[21] Drape J.L., Thelen P., Gay-Depassier P., Silbermann O., Benacerraf R., Intraarticular diffusion of Gd-DOTA after intravenous injection in knee MR imaging evaluation. Radiology 1993; 188:227-234.

[22] Edzes H.T., Samulski E.T., Crossrelaxation and spin diffusion in the proton NMR of hydrated collagen. Nature 1977; 265:521-523.

[23] Eleff S.M., Mclennan I.J., Hart G.K., Maruki Y., Traystman R.J., Koehler R.C., Shift reagent enhanced concurrent ^{23}Na and ^{1}H magnetic resonance spectroscopic studies of transcellular sodium distribution in dog brain in vivo. Magn Reson in Med 1993; 30:11-17.

[24] Eliav U., Navon G., Analysis of double quantum filtered NMR spectra of ^{23}Na in Biological Tissues. J Magn Reson 1994; 103:19-29.

[25] Erickson S.J., Prost R.W., Timins M.E., The magic angle effect: Background physics and clinical relevance. Radiology 1993; 188:23-25.

[26] Farndale R.W., Buttle D.J., Barrett A.J., Improved quantitation and discrimination of sulphated glycosaminoglycans by use of demethylmethylene blue. Biochim Biophys Acta 1986; 883:173-177.

[27] Farrar T.C., Pulse nuclear magnetic resonance spectroscopy. An introduction to the theory and applications. The Farragut Press Chicago Madison 1989.

[28] Foy B.D., Burstein D., Characteristics of extracellular sodium relaxation in perfused hearts with pathologic inetrventions. Magn Reson in Med 1992; 27:270-283.

[29] Freeman M.A.R., Adult articular cartilage. Grune & Stratton New York 1974.

[30] Fukushima E., Roeder S.B.W., Experimental Pulse NMR. A nuts and bolts approach. Addison-Wesley 1981.

[31] Ghelman B., Meniscal Tears of Knee: Evaluation by high-resolution CT combined with Arthrography. Radiology 1985; 157:23-27.

[32] Goldberg M., and Gilboa H., Sodium magnetic resonance in biological systems. Interpretation of the relaxation curves. Nuclear magnetic resonance spectroscopy in molecular biology ed by B. Pullman, D. Reidel, Publ. C. Holland 1978; 481-491.

[33] Granot J., Sodium Imaging by gradient reversal. J Magn Reson 1986; 68:575-581.

[34] Granot J., Sodium imaging of human body organs and extermities in vivo. Radiology 1988; 167:547-550.

[35] Grodzinsky A.J., Electromechanical and physiochemical properties of connective tissue. Cirt Rev Biobed Engr 1983; 9(2):133-199.

[36] Gylys-Morin V.M., Hajeck P.C., Sartoris D.J., Resnick D., Articular cartialge defects: Detectability in cadaver knees with MR. AJR 1987; 148:1153-1157.

[37] Hayes C.W., Sawyer R.W., Conway W.F., Patellar Cartilage Lesions: In vitro detection and staging with MR imaging and pathologic correlation. Radiology 1990; 176:479-483.

[38] Henderson B., Pettipher E.R., Murphy G., Metalloproteinases and cartilage proteoglycan depletion in chronic arthritis-comparison of antigen-induced and polycation-induced arthritis. Arthritis and Rheumatism 1990; 33:241-246.

[39] Herman L.J., Beltran J., Pitfalls in MR imaging of the knee. Radiology 1988; 167:775-781.

[40] Hilal S.K., Maudsley A.A., Ra J.B., Simon H.E., Roschmann P., Wittekoek S., Cho Z.H., Mun S.K., In vivo NMR imaging of sodium-23 in the human head. J Comput Assist Tomog 1985; 9(1):1-7.

[41] Hubbard P.S., Nonexponential nuclear magnetic relaxation by quadrupolar interaction. J Chem Phys 1970; 53:985-987.

[42] Jelicks L.A., Gupta R.K., Double quantum NMR of sodium ions in cells and tissues: Paramagnetic quenching of extracellular coherence. J Magn Reson 1989; 81:586-592.

[43] Jelicks L.A., Paul P.K., O'Byrne E., Gupta R.K., Hydrogen-1, sodium-23 and carbon-13 MR spectroscopy of cartilage degradation in vitro. JMRI 1993; 3:565-568.

[44] Konig H., Sauter R., Deimling M., Vogt M., Cartilage Disorders: Comparison of Spin echo, CHESS, and FLASH sequences with MR images. Radiology 1987; 164:753-758.

[45] Kundel H.L., Shetty A., Joseph P.M., Summers R.M., Kasseb E.A., Moore B., Sodium NMR imaging of lung water in rats. Magn Reson in Med 1988; 6:381-389 .

[46] Kusaka Y., Grunder W., Rumpel H., Dannhauer K.H., Gersonde K., MR microimaging of articular cartilage and contrast enhancement by manganese ions. Magn Reson in Med 1992; 24:137-148.

[47] Lai K.C., Henkelman M., Poon P.Y., Robenstein J., MR imaging of the knee. J Compu Assist Tomogr 1984; 8:1147-1154.

[48] Leigh J.S., Relaxation times in systems with chemical exchange: Some exact solutions. J Magn Reson 1971; 4:308-311.

[49] Lerner L., Torchia D.A., A multinecular NMR study of the interaction of cations with proteoglycans, Heparin and Ficoll. J Biol Chem 1986; 261(27):12706-12714.

[50] Lerner K.B., Rechl H.P., Gmeinweiser J.K., Henck A.F., Lukas H.P., Kohl H.P., Structure function and degeneration of bovine hayline cartilage: assessment with MR imaging in vitro. Radiology 1989; 170:495-499.

[51] Lesperance L.M., Gray M.L., Burstein D., Determination of fixed charge density in cartilage using nuclear magnetic resonance. J Ortho Res 1992; 10:1-13.

[52] Maroudas A., Muir H., Wingham J., The correlation of fixed negative charge with glycosaminoglycan content of human cartilage. Biochim Biophys Acta 1969; 177:492-500.

[53] Maroudas A., Thomas H., A simple physiochemical micromethod for determining fixed anionic groups in connective tissue. Biochim Biophys Acta 1970; 215:214-216.

[54] Maroudas A., Physiochemical properties of articular cartilage. Piman Medical, Kent England 1979; 215-290.

[55] Martinez D., Silvidi A.A., Stokes R.M., Nuclear Magnetic resonance studies of sodium ions in isolated frog muscle and liver. Biophys J 1969; 9:1256-1260.

[56] McDevitt C.A., Muir H., Biochemical changes in the cartilage of the knee in experimental and natural osteoarthritis in the dog. J of Bone Joint Surg 1976; 58-B:94-101.

[57] McLaughlin A.C., Leigh J.S., Relaxation times in systems with chemical exchange: Approximate solutions for the non dilute case. J Magn Reson 1973; 9:296-304.

[58] Mink J.H., Levy T, Crues III J.V., Tears of the anterior cruciate ligament and menisci of the knee: MR Imaging Evaluation. Radiology 1988; 167:769-774.

[59] Modl J.M., Sether L.A., Haughton V.M., Kneeland J.B., Articular cartilage: correlation of histologic zones with signal intensity at MR imaging. Radiology 1991; 181:853-855.

[60] Monoi H., Nuclaer magnetic resonance of tissue ^{23}Na correlation time. Biochim Biophys Acta 1976; 451:604-609.

[61] Monoi H., Uedaira H., Magnetic relaxation of ^{23}Na in heteregeneous systems. J Magn Reson 1980; 38:119-129.

[62] Nissen H., Jacobsen J.P., Horder M., Assessment of NMR visibility of intraerythrocytic sodium by flame photometric and ion competitive studies. Magn Reson in Med 1989; 10:388-398.

[63] Paul P.K., O'Byrne E., Blancuzzi V., Wilson D., Gunson D., Douglas F.L., Wang J.Z., Mezrich R.S., Magnetic resonance imaging reflects cartilage proteoglycan degradation in rabbit knee. Skeletal Radiology 1991; 20:31-36.

[64] Pekar J., Leigh J.S., Detection of biexponential relaxation in sodium-23 facilitated by double-quantum filtering. J Magn Reson 1986; 69:582-584.

[65] Perman W.H., Turski P.A., Houston L.W., Glover G.H>, Hayes C.E., Methodology of in vivo human sodium MR imaging at 1.5T. Radiology 1986; 160:811-820.

[66] Perman W.H., Thomasson D.M., Bernstein M.A., Turski P.A., Multiple short-echo (25ms) quantitation of in vivo sodium T_2 relaxation. Magn Reson in Med 1989; 9:153-160.

[67] Peterfy C.G., Majumdar S., Lang P., VanDijek C.F., Sack K., Genant H.K., MR imaging of arthritic knee: Improved discrimination of cartilage synovium and effusion with pulsed saturation transfer and fat suppressed T_1 weighted sequences. Radiology 1994; 191:413-419.

[68] Peto S., Gillis P., Henri V.P., Structure and dynamics of water in tendin from NMR relaxation measurements. Biophys J 1990; 57:71-84.

[69] Pettegrew J.W., Woessener D.E., Minshew N.J., Glonek T., Sodium-23 NMR analysis of human whole blood, erythrocytes and plasma, chemical shift, spin relaxation and intracellular sodium concentration studies. J Magn Reson 1984; 57:185-196.

[70] Pettegrew J.W., Post J.F.M., Panchalingam K., Withers G., Woessner D.E., ^{7}Li NMR study of normal human erythrocytes. J Magn Res 1987; 71:504-519.

[71] Pike M.M., Frazer J.C., Dedrick D.F., Ingwall J.S., Allen P.D., Sprnger C.S., Smith T.W., ^{23}Na and ^{39}K nuclear magnetic resonance studies of perfused rat hearts. Discrimination of intra- and extracellular ions using a shift reagent. Biophys J 1985; 48:159-173.

[72] Poole A.R., The growth plate: Cellular physiology, cartilage assembly and mineralization. Cartilage Molecular Aspects ed by Hall B. and Newman S. 1991; 179-211.

[73] Ra J.B., Hilal S.K., Oh C.H., Mun I.K., In vivo magnetic resonance imaging of sodium in human body. Magn Reson in Med 1988; 7:11-22.

[74] Ra J.B., Hilal S.K., Oh C.H., An algorothm for MR Imaging of the short T_2 fraction of sodium using the FID signal. J Comput Assist Tomog 1989; 13(2):302-309.

[75] Rechet M.P., Kramer J., Marcelis S., Pathria M.N., Trudell D., Haghighi P., Sartoris D.J., Resnick D., Abnormalities of articular cartilage in the knee: analysis of available MR techniques. Radiology 1993; 187:473-478.

[76] Reicher M.A., Rauschning W., Gold R.H., Bassett L.W., Lufkin R.B., Glen Jr. W., High-resolution magnetic resonance imaging of the knee joint: Normal Anatomy. AJR 1985a; 145:895-902.

[77] Reicher M.A., Bassett L.W., Gold R.H., High resolution magnetic resonance imaging of the knee joint: Pathologic correlations. AJR 1985b; 145:903-909.

[78] Rubenstein J.D., Kim J.K., Morava-Protzner I., Stanchev P.L., Henkelman R.M., Effects of collagen orientation on MR imaging characteristics of bovine articular cartilage . Radiology 1993; 188:219-226.

[79] Schuierer G., Ladbebck R., Barfub H., Hentschel D., Huk W.J., Sodium-23 imaging of supratentorial Lesions at 4.0T. Magn Reson in Med 1991; 22:1-9.

[80] Shimizu H., Effect of molecular shape on nuclear magnetic relaxation. II. Quadrupole relaxation. J Chem Phys 1964; 40(3):754-761.

[81] Shinar H., Navon G., NMR relaxation studies of intracellular Na^+ in red blood cells. Biophys Chem 1984; 20:275-283.

[82] Shinar H., Navon G., NMR relaxation studies of intracellular Na^+ in red blood cells and suspensions of nuclei. Biophys J 1991; 59:203-208.

[83] Shporer M., Civan M.M., Nuclear magnetic resonance of sodium-23 Linoleate-water. Basis for an alternative interpretation of sodium-23 spectra within cells. Biophys J 1972; 12:114-122.

[84] Shporer M., Civan M.M., Effects of trmperature and field strengths on the NMR relaxation times of ^{23}Na in frog striated muscle. Biochim biophys Acta 1974; 354:291-304.

[85] Slichter C.P., Principles of magnetic resonance. Springer-Verlag New York 1990.

[86] Stark D.D., Bradley W.G., Magnetic resonance imaging. Mosby year book 1992.

[87] Summers R.M., Joseph P.M., Renshaw P.F., Kundel H.L., Dextran-Magnetite: A contrast agent for sodium-23 MRI. Magn Reson Med 1988; 8:427-439.

[88] Venn M., Maroudas A., Chemical composition and swelling of normal and osteoarthrotic femoral head cartilage. I. Chemical composition. Ann Rheum Dis 1977; 36:121-129.

[89] Wilson D., Paul P.K., Robert D.E., Blancuzzi V., Gronlund-Jacob J., Vosbeck K., DiPasquale G., O'Byrne E.M., Magnetic resonance imaging and morphometric quantitation of cartilage histology afetr chronic infusion of interleukin-1 in rabbit knees. Proceedings society for experimental biology and medicine 1993; 203(1):30-37.

[90] Wossener D.E., Nuclear magnetic relaxation and structure in aqueous heterogeneous systems. Mol Phys 1977; 34:899-920.

[91] Woessner D.E., Relaxation theory with applications to biological studies. in NMR: Principles and applications to biomedical research. Springer-Varlag 1990.

[92] Yelin E., Arthritis: The cumulative impact of a common chronic condition. Arthritis and Rehumatism 1992; 35(5):489-497.

[93] Yulish B.S., Montanez J., Goodfellow D.B., Bryan P.J., Mulopulos G.P., Modic T.M., Chondromalacia patella: Assessment with MR images. Radiology 1987b; 164:763-766.